Published for SISSA by Springer

Received: July 5, 2021
Accepted: August 17, 2021
Published: September 6, 2021

Radiative decays of heavy-light mesons and the $f^{(T)}_{H,H^*,H_1}$ decay constants

Ben Pullin and Roman Zwicky

Higgs Centre for Theoretical Physics, School of Physics and Astronomy, University of Edinburgh, Edinburgh EH9 3JZ, Scotland

E-mail: b.pullin@ed.ac.uk, roman.zwicky@ed.ac.uk

Abstract: The on-shell matrix elements, or couplings $g_{HH^*(H_1)\gamma}$, describing the $B(D)^*_q \to B(D)_q\gamma$ and $B_{1q} \to B_q\gamma$ $(q = u, d, s)$ radiative decays, are determined from light-cone sum rules at next-to-leading order for the first time. Two different interpolating operators are used for the vector meson, providing additional robustness to our results. For the D^*-meson, where some rates are experimentally known, agreement is found. The couplings are of additional interest as they govern the lowest pole residue in the $B(D) \to \gamma$ form factors which in turn are connected to QED-corrections in leptonic decays $B(D) \to \ell\bar{\nu}$. Since the couplings and residues are related by the decay constants $f_{H^*(H_1)}$ and $f^T_{H^*(H_1)}$, we determine them at next-leading order as a by-product. The quantities $\{f^T_{H^*}, f^T_{H_1}\}$ have not previously been subjected to a QCD sum rule determination. All results are compared with the existing experimental and theoretical literature.

Keywords: NLO Computations, QCD Phenomenology

ArXiv ePrint: 2106.13617

Open Access, © The Authors.
Article funded by SCOAP[3].

https://doi.org/10.1007/JHEP09(2021)023

JHEP09(2021)023

Contents

JHEP09(2021)023

1 Introduction

In this paper, we consider the on-shell couplings $g_{HH^*\gamma}$ and $g_{HH_1\gamma}$, for $B(D)^*_q \to B(D)_q\gamma$ and $B_{1q} \to B_q\gamma$ where $q = u, d, s$, from light-cone sum rules (LCSR) [1, 2].[1] Our own interest in these couplings is two-fold. Firstly they describe the decay $H^*(H_1) \to H\gamma$; secondly they appear as residues of the $m^2_{H^*(H_1)}$-pole for the $H \to \gamma$ form factor e.g. [3]. The latter is of phenomenological importance for invisible particle searches, e.g. flavoured axion and dark photon in $B_s \to \ell\ell$ at the LHCb [4] and is indirectly related to QED-corrections to $H \to \ell\bar{\nu}$ as the pole is not far from the kinematic endpoint.

The results derive from the same correlation functions as the form factors but involve a double, rather than a single, dispersion relation. The additional dispersion variable is the momentum transfer of the form factor q^2 where the H^*, H_1-meson is the lowest lying state. This is a technically involved matter at next-to-leading order (NLO), and our computation provides the first complete NLO computation at twist-1 and -2 level, utilising the master integrals from [3, 5]. A notable aspect is that the kinetic mass scheme [6], gives more stable results than the $\overline{\text{MS}}$- and the pole-scheme.

The residues and the couplings differ, apart from ratios of known hadron masses, by decay constants (cf. section 2). We determine five distinct decay constants from local QCD sum rules (SRs) [7, 8] to ensure consistency of our results; the well-known pseudoscalar f_H and both the vector $f_{H^*}(f_{H_1})$ and tensor $f^T_{H^*}(f^T_{H_1})$ of the $1^-(1^+)$ state. To the best of our knowledge $\{f^T_{H^*}, f^T_{H_1}\}$ have not previously been determined from QCD SRs. A relevant feature is that some D^* couplings are known from experiment. This is not the case for the B^* as the unknown total width means that the coupling values cannot be inferred.

The $g_{H^*H\gamma}$ couplings have been considered in LCSR to LO in [9] and at NLO at twist-2 level [10]. Lattice determinations of $g_{D^*D\gamma}$ (with large uncertainty) [11] and $g_{D^*_sD_s\gamma}$ (with small uncertainty) [12] are available. Heavy-light meson decay constants have been evaluated to NLO (and partially beyond) in [13–15] in SR. Lattice results are numerous and include [16, 17].

The paper is organised as follows. In section 2 we define the couplings and give their relations to the residues of the form factors. Section 3 is concerned with the main SR aspects of the couplings e.g. the computation, the double dispersion relation and the Borel transform (with more detail in Appendices C and D). The main results for the residues and the couplings are given in tables 6 and 7 respectively. The decay constants, as bona fide predictions, are presented in section 4, with analytic results in appendix B. Numerical values of decay constants and ratios thereof are collected in tables 8 and 10 respectively. We conclude in section 5. Conventions, definitions and inputs are grouped into appendix A.

2 The couplings $g_{HH^*(H_1)\gamma}$ and their relation to $H \to \gamma$ form factors

The purpose of this section is to discuss relevant method-independent aspects of the computation. For concreteness we shall write $H = B$, throughout this section, which stands

[1] For the 1^+ state H_1 we only consider the B_1-state since the D_1-state is already overshadowed by the $D\pi\pi$ 3-particle state ($m_{D_1} - m_D - 2m_\pi \approx 270\,\text{MeV}$). This effect is less pronounced, as a result of m_c/m_b suppression, for the B_1 since $m_{B_1} - m_B - 2m_\pi \approx 160\,\text{MeV}$.

JHEP09(2021)023

for either of the beauty $B_{u,d,s}$- or charmed $D_{u,d,s}$-mesons. The couplings of interest are defined from the on-shell amplitudes[2]

$$\begin{aligned}\mathcal{A}_{B^*\to B\gamma} &= \frac{i}{2} s_e e\, \varepsilon^{\alpha\beta\gamma\delta} (p_B)_\alpha\, \eta_\beta\, F_{\gamma\delta}\; g_{BB^*\gamma}\,,\\ \mathcal{A}_{B_1\to B\gamma} &= -s_e e F_{\alpha\beta} (p_B)^\alpha \eta^\beta\, g_{BB_1\gamma}\,,\end{aligned} \tag{2.1}$$

where $D_\mu = \partial_\mu + ies_e A_\mu$ (with $s_e = \pm 1$ depending on convention), η is the vector meson's polarisation, $F_{\alpha\beta} = ik_{[\alpha}\epsilon^*_{\beta]}$ stands for the photon's outgoing plane wave and the coupling's mass dimension is $[g_{BB^*\gamma}] = [g_{BB_1\gamma}] = -1$. We refer the reader to appendix A for more details on conventions. For the decay rates, with $\alpha = e^2/4\pi$ as the fine structure constant, we obtain

$$\begin{aligned}\Gamma(B^* \to B\gamma) &= \frac{\alpha}{24}\left(1 - \frac{m_B^2}{m_{B^*}^2}\right)^3 m_{B^*}^3 g_{BB^*\gamma}^2\,,\\ \Gamma(B_1 \to B\gamma) &= \frac{\alpha}{24}\left(1 - \frac{m_B^2}{m_{B_1}^2}\right)^3 m_{B_1}^3 g_{BB_1\gamma}^2\,,\end{aligned} \tag{2.2}$$

where the first expression agrees with [18] for example. These rates follow from an effective Lagrangian of the form[3]

$$\mathcal{L}_{\text{eff}} = s_e g_{BB^*\gamma} \frac{1}{2}\epsilon(B^*, \partial B^\dagger, F) - i s_e g_{BB_1\gamma}\, B^*_\alpha \partial_\beta B^\dagger F^{\alpha\beta} + \text{h.c.}\,. \tag{2.3}$$

This Lagrangian can be used at small recoil and has to be supplemented by higher order couplings away from it.

As mentioned earlier, another point of interest in the couplings arises from their relation to pole-residues of the $\bar{B} \to \gamma$ form factors [3] (and cf. appendix A).[4] For clarity let us consider the dispersion representation of the vector form factor

$$V^{\bar{B}\to\gamma}_{\perp[\|]}(q^2) = \frac{1}{\pi}\int_{\text{cut}}^{\infty} dt \frac{\text{Im}[V^{\bar{B}\to\gamma}_{\perp[\|]}(t)]}{t - q^2 - i0} = \frac{r^V_{\perp[\|]}}{1 - q^2/m^2_{B^*[B_1]}} + \dots\,, \tag{2.4}$$

[2] More concretely the couplings parametrise the on-shell matrix elements $\langle \bar{B}(p_B)\gamma(k)|\bar{B}^*(q)\rangle = [-i(2\pi)^4\delta^{(4)}(\sum p_i)]\,\mathcal{A}_{B^*\to B\gamma}$ and $\langle \bar{B}(p_B)\gamma(k)|\bar{B}_1(q)\rangle = [-i(2\pi)^4\delta^{(4)}(\sum p_i)]\,\mathcal{A}_{B_1\to B\gamma}$.

[3] One might wonder whether the proximity of the B and B^* mass leads to any enhanced terms in the soft photon region in diagrams where the photon couples to an external B-meson and a lepton for instance (e.g. diagram top left of figure 3 in [19] where the weak Hamiltonian corresponds to $B^* \to K\ell\ell$). The behaviour of the denominator in the soft region (i.e. $k_\mu \to 0$), $\frac{1}{2k\cdot p_B + \Delta M_B^2}\frac{1}{k\cdot\ell_1}\frac{1}{k^2}$ with $\Delta M_B^2 = m_{B^*}^2 - m_B^2 = \mathcal{O}(m_b\Lambda_{\text{QCD}})$, is softened by the derivative term $F_{\alpha\beta}$ and avoids unsuppressed large logarithms of the form $\ln(\Delta M_B^2/m_B^2)$. This is another manifestation, with a different twist, of the finding in [19] (cf. section 3.4 therein) that structure dependent terms do not generate large logarithms.

[4] We note that when translating between the $\bar{B} \to \gamma$ and $B \to \gamma$ form factors only the axial, and not the vector parts change sign, as can be inferred by applying a charge C-transformation with $C|\bar{B}\rangle = |B\rangle$. We stress that our results are formally quoted for the $\bar{B}$-meson.

JHEP09(2021)023

where the dots represent higher terms in the spectrum. For the tensor form factor, $T_{\perp[\|]}^{\bar{B}\to\gamma}(q^2)$, the analogous form holds. The relation of the residues to the couplings are

$$r_\perp^V = \frac{m_B f_{B^*}}{m_{B^*}} g_{BB^*\gamma}\,, \qquad r_\perp^T(\mu_{\rm UV}) = f_{B^*}^T(\mu_{\rm UV}) g_{BB^*\gamma}\,,$$
$$r_\|^V = \frac{m_B f_{B_1}}{m_{B_1}} g_{BB_1\gamma}\,, \qquad r_\|^T(\mu_{\rm UV}) = f_{B_1}^T(\mu_{\rm UV}) g_{BB_1\gamma}\,, \tag{2.5}$$

with decay constants $f_{B^*(B_1)}^{(T)}$ defined in (3.7). The following exact relations, with $\mu_{\rm UV}$-dependence suppressed,

$$\frac{r_\perp^V}{r_\perp^T} = \frac{m_B f_{B^*}}{m_{B^*} f_{B^*}^T}\,, \quad \frac{r_\|^V}{r_\|^T} = \frac{m_B f_{B_1}}{m_{B_1} f_{B_1}^T}\,, \tag{2.6}$$

are a consequence of the freedom to choose a particle's interpolating operator in field theory. This provides us with a non-trivial consistency check of our SR evaluation. Finally a note on the ultraviolet (UV) scale dependence $\mu_{\rm UV}$. The couplings are of course scale-independent since they correspond to on-shell matrix elements. Thus the vector residues are scale-independent whereas the tensor ones scale like the tensor decay constant

$$\gamma_T = -\frac{d}{d\ln\mu_{\rm UV}} \ln f_{B^*(B_1)}^T(\mu_{\rm UV}) = -\frac{d}{d\ln\mu_{\rm UV}} \ln r_{\perp(\|)}^T(\mu_{\rm UV})\,, \tag{2.7}$$

with

$$\gamma_T = \frac{\alpha_s}{4\pi} 2C_F + O(\alpha_s^2)\,, \tag{2.8}$$

and $C_F = (N_c^2-1)/(2N_c) = 4/3$.

3 The $g_{HH^*(H_1)\gamma}$ couplings from light-cone sum rules

3.1 The computation

The couplings can be computed within the framework of QCD SRs on the light-cone. Proceeding via standard techniques we define two correlation functions [3]

$$\Pi_{\perp\mu}^\Gamma(p_B,q) \equiv i\int_x e^{-ip_B\cdot x}\langle\gamma(k,\epsilon)|TJ_{B_q}(x)O_{\perp\mu}^\Gamma(0)|0\rangle = s_e P_\mu^\perp\,\Pi_\perp^\Gamma(p_B^2,q^2)\,, \tag{3.1}$$
$$\Pi_{\|\mu}^\Gamma(p_B,q) \equiv i\int_x e^{-ip_B\cdot x}\langle\gamma(k,\epsilon)|TJ_{B_q}(x)O_{\|\mu}^\Gamma(0)|0\rangle = s_e\left(-P_\mu^\|\,\Pi_\|^\Gamma(p_B^2,q^2)+\dots\right),$$

with quantum numbers chosen such that $\Pi_\perp^\Gamma$ and $\Pi_\|^\Gamma$ contain information on $g_{BB^*\gamma}$ and $g_{BB_1\gamma}$, respectively and $\Gamma\in\{V,T\}$. Above the shorthand $\int_x = \int d^4x$ has been adopted and the dots represent structures [3] which are not important for this discussion. The B-meson is interpolated by the operator J_{B_q}

$$J_{B_q} \equiv (m_b+m_q)\bar{b}i\gamma_5 q\,, \quad \langle\bar{B}_q|J_{B_q}|0\rangle = m_{B_q}^2 f_{B_q}\,, \tag{3.2}$$

and the Lorentz structures $P_{\perp,\|}^\mu$ are given by

$$P_\mu^\perp \equiv \varepsilon_{\mu\rho\beta\gamma}\epsilon^{*\rho}(p_B)^\beta k^\gamma\,, \quad P_\mu^\| \equiv i\,(p_B\cdot k\,\epsilon_\mu^* - p_B\cdot\epsilon^*\,k_\mu)\,, \tag{3.3}$$

JHEP09(2021)023

with ϵ the photon's polarisation vector, $p_B = q + k$ and on-shell momentum $k^2 = 0$. The vector and tensor operators of the $b \to q$ effective Hamiltonian are given by

$$O^V_{\perp\mu} \equiv -\frac{1}{e} m_{B_q} \bar{q} \gamma_\mu b\,, \qquad O^T_{\perp\mu} \equiv \frac{1}{e} \bar{q} i q^\nu \sigma_{\mu\nu} b\,,$$
$$O^V_{\parallel\mu} \equiv \frac{1}{e} m_{B_q} \bar{q} \gamma_\mu \gamma_5 b\,, \qquad O^T_{\parallel\mu} \equiv \frac{1}{e} \bar{q} i q^\nu \sigma_{\mu\nu} \gamma_5 b\,. \tag{3.4}$$

For brevity, from this point onwards we drop the subscript denoting the quark flavour such that $m_{B_q} = m_B$, $f_{B_q} = f_B$, et cetera. As previously mentioned, the computation of the correlation function is the same as for the $\bar{B} \to \gamma$ form factor; we refer the reader to [3] for details of the calculation and now turn to the double dispersion relation.

3.2 The dispersion relation

The hadronic representation of the correlation functions is obtained from the double discontinuity of the correlation function[5]

$$\rho^\Gamma_{\text{had}^*}(p_B^2, q^2) = \frac{1}{(2\pi i)^2} \text{disc}_{q^2} \text{disc}_{p_B^2} \Pi^\Gamma_\perp(p_B^2, q^2)\,, \tag{3.5}$$

and reads

$$s_e \Pi^\Gamma_{\perp\mu} = \sum_{\text{pol}} \frac{\langle 0|J_B|\bar{B}\rangle \mathcal{A}_{B^*\to B\gamma} \langle \bar{B}^*|O^\Gamma_{\perp\mu}|0\rangle}{(m^2_{B^*} - q^2)(m^2_B - p_B^2)} + P^\perp_\mu \iint_{\Sigma_\perp} ds\, dt \frac{\rho^\Gamma_{\text{had}^*}(s,t)}{(t-q^2)(s-p_B^2)} + \ldots,$$
$$s_e \Pi^\Gamma_{\parallel\mu} = \sum_{\text{pol}} \frac{\langle 0|J_B|\bar{B}\rangle \mathcal{A}_{B_1\to B\gamma} \langle \bar{B}_1|O^\Gamma_{\parallel\mu}|0\rangle}{(m^2_{B_1} - q^2)(m^2_B - p_B^2)} - P^\parallel_\mu \iint_{\Sigma_\parallel} ds\, dt \frac{\rho^\Gamma_{\text{had}_1}(s,t)}{(t-q^2)(s-p_B^2)} + \ldots, \tag{3.6}$$

where the sum runs over the vector meson's polarisations. The integration domain $\Sigma_{\perp,\parallel}$ ranges from a lower cut shifted by two pion masses from the poles up to infinity. The dots indicate single dispersion integrals which do not contribute to the final result, and can be seen as the analogues of the subtraction terms of single dispersion integrals.

The matrix elements to the right are the decay constants

$$\langle 0|(O^V_{\perp\mu})^\dagger|\bar{B}^*\rangle = -\frac{1}{e} m_B m_{B^*} f_{B^*} \eta_\mu\,, \qquad \langle 0|(O^T_{\perp\mu})^\dagger|\bar{B}^*\rangle = -\frac{1}{e} m^2_{B^*} f^T_{B^*} \eta_\mu\,,$$
$$\langle 0|(O^V_{\parallel\mu})^\dagger|\bar{B}_1\rangle = \frac{1}{e} m_B m_{B_1} f_{B^*} \eta_\mu\,, \qquad \langle 0|(O^T_{\parallel\mu})^\dagger|\bar{B}_1\rangle = \frac{1}{e} m^2_{B_1} f^T_{B_1} \eta_\mu\,, \tag{3.7}$$

where η is the vector mesons' polarisation vector e.g. eq. (A.2). The SR procedure involves the Borel transformation in both variables, $\Pi^\Gamma_{\parallel[\perp]}(M_1^2, M_2^2) \equiv \mathcal{B}^{q^2}_{M_2^2} \mathcal{B}^{p_B^2}_{M_1^2} \Pi^\Gamma_{\parallel[\perp]}(p_B^2, q^2)$, to enhance convergence. In the case of a dispersion relation of the form (3.6) this is straightforward due to the well-known formula

$$\mathcal{B}^{q^2}_{M^2}\left(\frac{1}{m^2 - q^2}\right) = e^{-m^2/M^2}\,. \tag{3.8}$$

We refer the reader to appendix D for the definition of the Borel transformation.

[5] As Schwartz's reflection principle applies, one may use Disc $\to 2i$ Im cf. [20] for instance.

JHEP09(2021)023

3.3 The light-cone operator product expansion

The correlation functions (3.1) are evaluated with perturbative QCD using the light-cone operator product expansion (LC-OPE) ordered, in practice, by a converging expansion in twist. The twist, known from deep inelastic scattering, is the dimension of the operator minus its spin. We refer to [3] for specific details and to the technical [21] and applied [2] reviews on the subject. It seems worthwhile to state that, contrary to intuition, the photon is more involved than an ordinary vector meson as it has both perturbative (twist-1) *and* non-perturbative nature (higher-twist). The latter is encoded in the photon distribution amplitude (DA) which can be understood as ρ/ω-γ or ϕ-γ conversions. At LO in α_s we perform the computation up to twist-4 including 3-particle DAs, whilst at next-to-LO (NLO) twist-1 and twist-2 contributions have been computed. See however section 3.5 for remarks on the completeness of twist-4.

3.3.1 The "partonic" dispersion relation

One may also write a dispersion relation in perturbative QCD,

$$\Pi^{\Gamma}_{\parallel[\perp]}(p_B^2, q^2) = \int_{m_b^2}^{\infty} ds \int_{m_b^2}^{\infty} dt \frac{\rho^{\Gamma}_{\parallel[\perp]}(s,t)}{(t-q^2)(s-p_B^2)} + \dots \tag{3.9}$$

which is formally distinct by its slightly different analytic structure with the discontinuity starting at m_b^2.[6] The dots have the same meaning as for the "hadronic" dispersion relation.

Performing the double dispersion relation at NLO is complicated by pole singularities in $q^2 = p_B^2$. Taking a single discontinuity, say in p_B^2, one is faced with

$$\mathrm{disc}_{p_B^2} \Pi^{\Gamma}_{\perp}(p_B^2, q^2) = \sum_{n=0}^{3} \frac{\rho_i(q^2, p_B^2)}{(q^2 - p_B^2)^n}\,, \tag{3.10}$$

where the ρ_i themselves contain non-trivial cuts.[7] These singularities, dubbed second type singularities [20, 22], are solutions of the Landau equation for $\Pi^{\Gamma}_{\perp}(p_B^2, q^2)$ but are not on the physical sheet. However this changes once the discontinuity is taken in p_B^2 and they need to be taken into account. We refer the reader to appendix C for technical details.[8]

3.3.2 Borel transformation of LO terms for generic distribution amplitudes

As previously stated, for a given dispersion representation (3.9) the Borel transformation is straightforward due to (3.8). However, this demands committing to a specific DA. As

[6] The $m_{u,d,s}$ masses are considered in the linear approximation for which we have derived new results such as the m_q-correction to the twist-2 photon DA [3].

[7] At LO this is not the case and this is what makes them considerably easier to handle in practice.

[8] An alternative is to use Schwartz's reflection principle, Disc $\to 2i\,\mathrm{Im}$, to obtain the discontinuity cf. footnote 5. One can then deform the dt-integration path into the complex plane, away from the poles, in order to obtain a working dispersion representation. This approach, whilst being computationally inefficient, provides numerically stable results as long as the upper integration boundaries in the dt and ds integrals are sufficiently far apart. However, given the almost degenerate values of the masses m_B and m_{B^*} a sufficient separation of the upper boundaries can not be justified, rendering this approach sub-optimal.

JHEP09(2021)023

these can improve over time, due to better determination of hadronic parameters, there is some advantage in keeping them generic. Let us consider

$$\Pi(p_B^2, q^2) \supset \int_0^1 du \frac{(q^2)^\ell f_n(u)}{(m_b^2 - u p_B^2 - \bar{u} q^2)^n}\,, \quad \ell = 0, 1\,, \quad n = 1, 2, 3\,, \tag{3.11}$$

where $f_n(u)$ is some function proportional to the DA with suitable features in order to be compatible with first principle analytic properties. How to perform the Borel transformation *and* the continuum subtraction is described in appendix D. These results extend those currently seen in the literature and are presented in greater detail. In theory a double Borel transform provides two Borel parameters. In practice however, we content ourselves to setting them equal

$$M_1^2 = M_2^2 = 2\bar{M}^2 \to 2\hat{M}^2\,, \tag{3.12}$$

(and $u_0 = 1/2$ cf. (D.12)), which is justified since $m_B \approx m_{B^*} (\approx m_{B_1})$. The 3-particle DAs can be handled with the same technique as they reduce to an effective 2-particle DA (cf. appendix D in reference [3]).

3.4 The sum rule

The final step in completing the SR is to invoke semi-global quark-hadron duality. For a double dispersion relation this is not straightforward. Before addressing this issue let us assume an integration region (parametrised by a single parameter a and $\bar{\delta}_{s,t}^{(a)}$ specified in the next subsection), implemented with step function on the spectral density

$$\rho^\Gamma_{\text{had}_1[\text{had}^*]}(s,t) = \rho^\Gamma_{\|[\perp]}(s,t)\Theta(s - \bar{\delta}_s^{(a)}(m_b^2))\Theta(t - \bar{\delta}_t^{(a)}(s))\,. \tag{3.13}$$

Equating the"partonic" and "hadronic" parts one obtains the sum rule

$$f_B r^\Gamma_{\|[\perp]} = \frac{1}{m_B^2 m^2_{B_1[B^*]}} \int_{m_b^2}^{\bar{\delta}_s^{(a)}(m_b^2)} ds \int_{m_b^2}^{\bar{\delta}_t^{(a)}(s)} dt\, e^{\frac{m_B^2 - s}{2\bar{M}^2}} e^{\frac{m^2_{B_1[B^*]} - t}{2\bar{M}^2}} \rho^\Gamma_{\|[\perp]}(s,t)\,, \tag{3.14}$$

with the relation between the couplings and the residues $r^\Gamma_{\|[\perp]}$ given in (2.5) and $\Gamma = V, T$. The somewhat unconventional factor of two in the exponent is a consequence of our definition of the Borel mass (3.12). The LCSR determines the product $f_B r^\Gamma_{\|[\perp]}$ and to obtain the residues and the couplings one replaces the decay constants by a QCD SR to the same accuracy in α_s, e.g.

$$r^\Gamma_{\|[\perp]} = \frac{[f_B r^\Gamma_{\|[\perp]}]_{\text{LCSR}}}{[f_B]_{\text{SR}}}\,, \tag{3.15}$$

and

$$\begin{aligned} g_{BB^*\gamma} &= \frac{m_B^*}{m_B} \frac{[f_B r^V_{\|[\perp]}]_{\text{LCSR}}}{[f_B]_{\text{SR}}[f_{B^*}]_{\text{SR}}} = \frac{[f_B r^T_{\|[\perp]}]_{\text{LCSR}}}{[f_B]_{\text{SR}}[f^T_{B^*}]_{\text{SR}}}\,, \\ g_{BB_1\gamma} &= \frac{m_{B_1}}{m_B} \frac{[f_B r^V_{\|[\perp]}]_{\text{LCSR}}}{[f_B]_{\text{SR}}[f_{B_1}]_{\text{SR}}} = \frac{[f_B r^T_{\|[\perp]}]_{\text{LCSR}}}{[f_B]_{\text{SR}}[f^T_{B_1}]_{\text{SR}}}\,. \end{aligned} \tag{3.16}$$

As previously mentioned, the two determinations for each couplings serve as an additional quality test of our SR.

JHEP09(2021)023

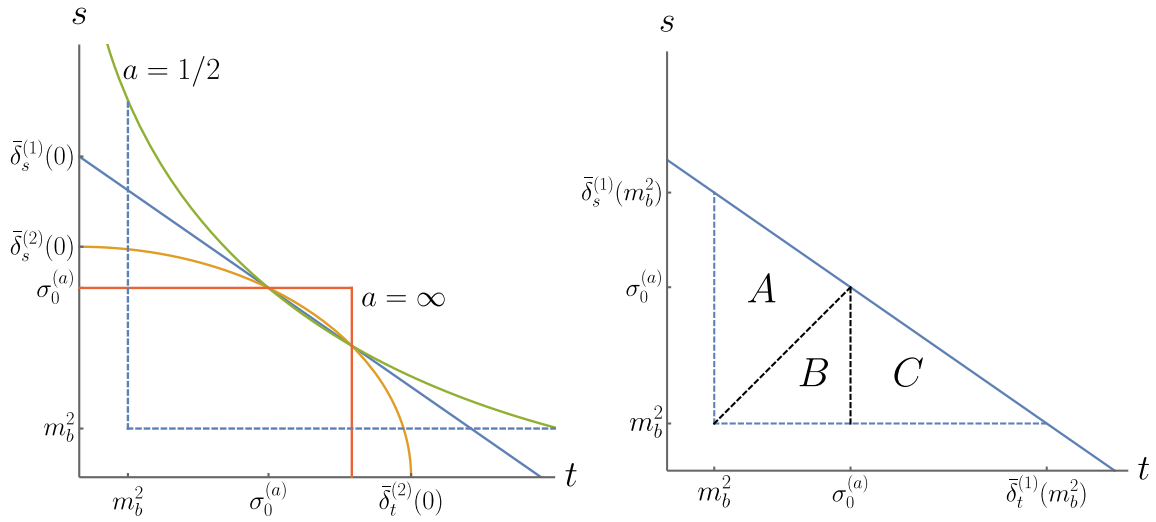

Figure 1. An overview of the duality interval. The left hand figure demonstrates how the parameterisation (3.17), keeping the quantity $\sigma_0^{(a)}$ fixed, leads to a range of possible duality windows depending on the value of the parameter a. The solid green, blue, yellow, and orange curves correspond to the $a = 1/2, 1, 2, \infty$, cases respectively. In the limit $\tilde{s}_0 \to \tilde{t}_0$ the curves intersect at a single point, $\sigma_0^{(a)}$. The right hand plot provides a more detailed view of the case $a = 1$, which we adopt for our evaluation of the couplings. We note that the choice of duality window has little impact on the final result, cf. table 5. The dashed blue line indicates the lower boundary on the duality window, enforced by the restriction that both t and s can only take values above the cut starting at m_b^2. The dashed black line indicates a technical division of the duality region necessary for application of the principal part prescription, cf. (C.8).

3.4.1 Duality region as a function of the duality parameter a

Finally we turn to the question of the duality region encoded in (3.13) and derive explicit relations as a function of the parameter a. In defining the duality region,

$$\left(\frac{s}{\tilde{s}_0}\right)^a + \left(\frac{t}{\tilde{t}_0}\right)^a \leq 1\,, \tag{3.17}$$

we follow earlier work [1, 23] but extend it in that we consider $\tilde{s}_0, \tilde{t}_0$ as a function of the parameter a. The solutions to the boundary defined by (3.17), and which therefore enter (3.13), are

$$\bar{\delta}_s^{(a)}(t) = \tilde{s}_0 \left(1 - \left(\frac{t}{\tilde{t}_0}\right)^a\right)^{1/a}\,, \quad \bar{\delta}_t^{(a)}(s) = \tilde{t}_0 \left(1 - \left(\frac{s}{\tilde{s}_0}\right)^a\right)^{1/a}\,. \tag{3.18}$$

A further quantity that arising from the parameterisation, and thus appearing in results given in the appendix, is

$$\sigma_0^{(a)} = \frac{\tilde{s}_0 \tilde{t}_0}{(\tilde{s}_0^a + \tilde{t}_0^a)^{1/a}}\,. \tag{3.19}$$

Its geometric meaning can be inferred from figure 1. It takes on the rôle of the single dispersion effective threshold if $\rho^\Gamma \propto \delta(s-t)$ which is the case for a large part of the contributions. Fortunately, variation of the duality parameter a does not lead to large

JHEP09(2021)023

effects when the daughter sum rule is invoked to constrain the SR parameters, as will be discussed in the next section.

We turn to the question of which choice of the parameter a is suitable. We find that in the majority of cases the dependence of the couplings on the duality window is rather limited, as evidenced by table 5. The exceptions are the B_{1s}- and the D_s^*-meson cases, showing more significant variation. It has been argued that for the Isgur-Wise function [24] and the small velocity limit [25] that $a = 1$ is a necessary choice. Whether or not this translates to other cases and in particular to the case at hand is an open question. We adopt $a = 1$ as our default choice, and include variations under the duality window in our estimate of the total uncertainty (cf. section 3.5.1).

3.5 Numerical analysis

Physical input parameters used for the numerical evaluation of the SRs can be found in table 14 in the appendix.

As there are a number of different renormalisation scales involved we discuss them in some detail. The UV scale, $\mu_{\rm UV}$, has already been mentioned below eq. (2.6) and is set to the pole mass $m_b(m_c)^{\rm pole}$. For the LCSR there remains the scale of the coupling μ_{α_s}, the mass μ_m (or $\mu_{\rm kin}$ cf. below) and the LC-OPE factorisation scale μ_F. We set $\mu_F^2 = m_B^2 - (m_b^{\rm kin}(1\,{\rm GeV}))^2 (= m_D^2 - m_c^2(m_c))$ which is a standard albeit not a necessary choice and equate $\mu_{\alpha_s} = \mu_F$. The choice of a mass scale is linked with a choice of mass scheme. For the $B \to \gamma$ form factors we have found [3] that the $\overline{\rm MS}$- and the pole-scheme give rise to large effects in either higher twist or at $\mathcal{O}(\alpha_s)$ rendering both of them suboptimal. For the $g_{BB^*(B_1)\gamma}$ couplings the evidence for adopting the kinetic- over the $\overline{\rm MS}$-scheme is less compelling (smaller improvement in twist-convergence). However, in an effort to remain consistent with our previous work [3], we choose to adopt the kinetic-scheme for the evaluation of both the FF residues and the effective couplings. As the kinetic mass scheme, originally devised for the inclusive decay operator product expansion (OPE) [6], can be considered as a compromise between the $\overline{\rm MS}$- and the pole-scheme. Moreover, it is indeed found that the kinetic scheme is stable under scale variation. The kinetic scale is set to $\mu_{\rm kin} = 1\,{\rm GeV}$, with further details in [3]. For the D-meson decays the situation is different and the $\overline{\rm MS}$ scheme gives more stable results than the kinetic scheme and we thus employ the $\overline{\rm MS}$ scheme with the standard choice $\mu_m = m_c(m_c)$. This might not come as a surprise since m_c itself is closer to μ_F as compared to the B-case.

As indicated in eqs. (3.15) and (3.16), to obtain the physical quantities one needs to divide by the decay constant(s) to the same order (cf. section 4 for their discussion). The new inputs are the condensates, given in table 14, and the factorisation scale of the local OPE, denoted by $\mu_{\rm cond}$, which is set to $\mu_{\rm cond} = \mu_F$ in order to facilitate cancellations in the ratio. A summary of all renormalisation scales is given in table 1 (left). Another aspect is that we drop twist-4 corrections, other than the pure quark condensates, as they are incomplete (requiring the inclusion of 4-particle DAs [3]). The resulting uncertainty ought to be captured, at least in part, by the variation of the Borel parameter.

The SR parameters $\{\sigma_0^{(a)}, \hat{M}^2\}$ and $\{s_0^{f_B}, M_{f_B}^2\}$ are determined by a number of constraints. As usual the Borel mass is determined subject to two competing factors, contami-

JHEP09(2021)023

		$\mu_F^2=\mu_{\alpha_s}^2=\mu_{\rm cond}^2[\,{\rm GeV}^2]$	$\mu_{\rm UV}[\,{\rm GeV}]$	$\mu_m[\,{\rm GeV}]$	$\mu_{\rm kin}[\,{\rm GeV}]$	$\mu_{\alpha_s}[\,{\rm GeV}]$	$\mu_{\rm cond}[\,{\rm GeV}]$
B	Kin	$m_B^2-(m_b^{\rm pole})^2$	4.78(1.0)	–	1.0(4)	4.18(1.5)	3.0(1.0)
B	$\overline{\rm MS}$	$m_B^2-(m_b^{\rm pole})^2$	4.78(1.0)	$4.18^{+1.7}_{-1.2}$	–	4.18(1.5)	3.0(1.0)
D	$\overline{\rm MS}$	$m_D^2-m_c(m_c)^2$	1.67(30)	$1.27^{+1.5}_{-0.2}$	–	$1.27^{+1.0}_{-0.2}$	2.0(1.0)

Table 1. Summary of the scales involved in the determination of the residues (table 6) and coupling constants (table 7) to the left of the double separation line. To the right we have the scale changes used for the best determination of the decay constants (table 8). The quantity $m_c(m_c)$, above, is the $\overline{\rm MS}$ mass at the scale m_c. The uncertainty in μ_F, for the B-meson (D-meson), is chosen to be $\Delta\mu_F=\pm1\,{\rm GeV}$ ($\Delta\mu_F=^{+1.0}_{-0.2}$ GeV).

nation from higher states is effectively suppressed by a small $\hat{M}^2$, whilst fast convergence of the LC-OPE favours a large $\hat{M}^2$ as higher terms in the expansion are accompanied by ever increasing inverse powers of the Borel mass. The compromise of these two criteria, resulting in an approximately flat curve, is known as the Borel-window. To constrain the effective thresholds $\{\tilde{s}_0,\tilde{t}_0\}$ the, formally exact, daughter SR for the sum of meson masses (3.20) is employed

$$m_B^2+m_{B_1[B^*]}^2=2\hat{M}^4\frac{d}{d\hat{M}^2}\ln\int_{m_b^2}^{\tilde{\delta}_s^{(a)}(m_b^2)}ds\int_{m_b^2}^{\tilde{\delta}_t^{(a)}(t)}dt\,e^{-\frac{s+t}{2\hat{M}^2}}\,\rho^{\Gamma}_{[\parallel\perp]}(s,t)\,, \tag{3.20}$$

with the ratio of $\tilde{s}_0,\tilde{t}_0$ matched to the ratio of meson masses in the respective channels cf. caption of table 2. In addition we impose $\tilde{s}_0^{B_s}/\tilde{s}_0^{B_{d,u}}\approx m_{B_s}^2/m_{B_{d,u}}^2$ and $s_0^{f_B}/s_0^{f_{B^*[B_1]}}\approx m_B^2/m_{B^*[B_1]}^2$ to be satisfied reasonably well. We turn to the dependency on a specific duality parameter a. It is found that in the B-meson cases a single set of SR parameters is sufficient to satisfy (3.20) to within $\approx2\%$ for the $a=\{1/2,1,2\}$ cases considered. For the D-mesons this no longer holds and a small modification to the SR parameters is made at each value of a.

We consider it worthwhile to comment on the specific numerical values of the thresholds found. The expectation for a single dispersive threshold s_0 is $(m_{B_i}+2m_\pi)^2<s_0<(m_{B_i}+m_\rho)^2$, and lying closer to the top boundary. Inspecting table 2, we note that this is indeed the case for the single dispersion threshold $s_0^{f_B}$ but not for the double dispersion threshold $\sigma_0^{(a)}$ (3.19). Whereas $\sigma_0^{(a)}$ takes on a similar rôle to the single dispersive effective threshold, one must remember that it contains additional information on the excited vector meson channel, cf. (3.18) and might further be a result of the peculiar analytic structure in (s,t) of the LC-OPE.[9]

Let us turn to the correlation imposed on parameters based on physical arguments. Whilst the effective threshold for decay constant $s_0^{f_B}$ can be independently determined it would contradict the method if it were completely independent of the $\sigma_0^{(a)}$-threshold, since they are both associated with the same state. A 50%-correlation is adopted between the two. The vector versus tensor results are correlated since, by the (exact) equation of

[9]It is conceivable that if one were to adapt the daughter sum rule method to the extraction of $g_{DD*\pi}$ and $g_{BB^*\pi}$ in [23], one could even find better agreement with experiment and/or the lattice.

JHEP09(2021)023

SR parameters [GeV^2]

	B_d	B_s	B_u		$B_{d,u}$	B_s
$\{\sigma_0^{(a)}, \hat{M}^2\}^{r_\perp^V, r_\perp^T}$	37.7, 8.0	39.2, 11.0	37.7, 8.0	$\{s_0, M^2\}^{f_B}$	34.3, 5.6	35.5, 6.4
$\{\sigma_0^{(a)}, \hat{M}^2\}^{r_\parallel^V}$	43.5, 12.0	45.5, 13.5	43.5, 12.0	$\{s_0, M^2\}^{f_{B^*}, f_{B^*}^T}$	34.5, 5.7	35.9, 7.1
$\{\sigma_0^{(a)}, \hat{M}^2\}^{r_\parallel^T}$	42.5, 11.0	44.4, 13.5	42.5, 11.0	$\{s_0, M^2\}^{f_{B_1}, f_{B_1}^T}$	38.9, 6.0	40.6, 8.6
	D_d	D_s	D_u		$D_{d,u}$	D_s
$\{\sigma_0^{(1/2)}, \hat{M}^2\}^{r_\perp^V}$	5.9, 3.1	6.6, 3.4	5.9, 3.1	$\{s_0, M^2\}^{f_D}$	5.7, 1.9	6.3, 2.2
$\{\sigma_0^{(1/2)}, \hat{M}^2\}^{r_\perp^T}$	5.9, 2.6	6.6, 2.9	5.9, 2.6	$\{s_0, M^2\}^{f_{D^*}, f_{D^*}^T}$	6.1, 1.9	6.9, 2.6
$\{\sigma_0^{(1)}, \hat{M}^2\}^{r_\perp^V}$	6.0, 2.9	6.7, 3.2	6.0, 2.9			
$\{\sigma_0^{(1)}, \hat{M}^2\}^{r_\perp^T}$	6.0, 2.4	6.7, 2.7	6.0, 2.4			
$\{\sigma_0^{(2)}, \hat{M}^2\}^{r_\perp^V}$	5.7, 2.9	6.5, 3.4	5.7, 2.9			
$\{\sigma_0^{(2)}, \hat{M}^2\}^{r_\perp^T}$	5.7, 2.4	6.5, 2.7	5.7, 2.4			

Table 2. Summary of the SR parameters used in the determination of the residues for the triangular duality window $a = 1$ (cf. section 3.5.1 for comments). The additional threshold parameter is fixed via the ratio of the scalar and vector mesons. For the B-mesons $\tilde{t}_0/\tilde{s}_0 = m_{B^*}^2/m_B^2 \approx 1.02$ and $\tilde{t}_0/\tilde{s}_0 = m_{B_1}^2/m_B^2 \approx 1.18$ in the $\perp$ and $\parallel$ directions respectively. In the D-meson channels $\tilde{t}_0/\tilde{s}_0 = m_{D^*}^2/m_D^2 \approx 1.15$. Note the difference between the values of $\sigma_0^{(a)}$ for the $\perp$- and $\parallel$-directions reflects the fact that $m_{B_1}^2/m_{B^*}^2 \approx 1.16$. We remind the reader that in the B-meson channels a single set of SR parameters is sufficient to satisfy the daughter SR (3.20) to within $\approx 2\%$ for all three choices of the duality parameter a. For the B-meson (D-meson) processes we associate a uniform uncertainty to the threshold of $\pm 2.0\,\mathrm{GeV}^2$ ($\pm 0.5\,\mathrm{GeV}^2$) and the Borel mass of $\pm 2.0\,\mathrm{GeV}^2$ ($\pm 0.5\,\mathrm{GeV}^2$).

motion, their difference is equal to a derivative operator which is numerically (and to some extent parametrically) suppressed at low recoil. In order to remain consistent this implies a correlation of the effective thresholds, as argued in [26] and more systematically exploited in [27].[10] The correlations

$$\mathrm{corr}\left(\sigma_0^{(a)V_\perp}, \sigma_0^{(a)T_\perp}\right)|_B = \frac{4}{5}, \quad \mathrm{corr}\left(\sigma_0^{(a)V_\parallel}, \sigma_0^{(a)T_\parallel}\right)|_B = \frac{1}{2}, \quad \mathrm{corr}\left(\sigma_0^{(a)V}, \sigma_0^{(a)T}\right)|_D = \frac{2}{3}, \tag{3.21}$$

are imposed based on the contribution of the derivative operator to the equations of motion, which is $\approx 10\%$ in the B $\perp$- and $\approx 20\%$ in the D $\perp$-case. In the $B\parallel$-case the contribution is $\approx$ 40–45%.

Another relevant aspect concerning the plethora of predictions is that not all channels are of equal quality. This is highlighted by the two separate determinations of the residue, from the vector and tensor interpolating current. Let us define the ratio $U_{B^{(i)}} = g_{BB^{(i)}\gamma}^T / g_{BB^{(i)}\gamma}^V$ which ideally is close to one. We find reassur-

[10] However, for the $\parallel$-direction the derivative term is not small and such a correlation does not make sense. See section 4.2 in [3] for a more elaborate discussion in the context of the $\bar{B} \to \gamma$ form factors.

JHEP09(2021)023

ingly good values for the B^*-case $(U_{B^{*0}}, U_{B_s^*}, U_{B^{*+}}) = (0.99, 0.98, 0.98)$, moderate deviations $(U_{D^{*+}}, U_{D_s^*}, U_{D^{*0}}) = (0.81, 0.82, 0.91)$ for the D^*-case and significant deviations $(U_{B_1^0}, U_{B_{1s}}, U_{B_1^+}) = (1.35, 1.26, 1.30)$ for the B_1-case as anticipated cf. footnote 1. For the D^*-case it is the accidental cancellation of the two charge contributions in perturbation theory, to be discussed further below, and the sensitivity to higher twist which gives rise to larger deviation from one. For the B_1-case the concept of a well isolated resonance is not assured and for the D_1 it simply does not hold cf. also footnote 1. Therefore we do not quote any results for the D_1 whilst for the B_1 the results are deemed just marginally acceptable to present.

It is instructive to present a breakdown in terms of charges for comparison with other work and illustrate the, presumably accidental, cancellations in the charged D- and B_1-case which unfortunately implies that these results are less reliable. For definiteness we quote the breakdown for the couplings obtained from the *vector* interpolating current

$$\begin{aligned}
g_{D_q D_q^* \gamma} &\approx -(1.05\, Q_q + 0.51\, Q_c)|_{\text{PT}} - 1.74\, Q_q|_{\text{twist-2}} + \text{ht}\,, \\
g_{D_s D_s^* \gamma} &\approx -(1.24\, Q_s + 0.51\, Q_c)|_{\text{PT}} - 1.62\, Q_s|_{\text{twist-2}} + \text{ht}\,, \\
g_{B_q B_q^* \gamma} &\approx -(1.20\, Q_q + 0.24\, Q_b)|_{\text{PT}} - 1.20\, Q_q|_{\text{twist-2}} + \text{ht}\,, \\
g_{B_s B_s^* \gamma} &\approx -(1.31\, Q_s + 0.25\, Q_b)|_{\text{PT}} - 1.10\, Q_s|_{\text{twist-2}} + \text{ht}\,, \\
g_{B_q B_{1q} \gamma} &\approx +(0.12\, Q_q + 0.02\, Q_b)|_{\text{PT}} - 1.11\, Q_q|_{\text{twist-2}} + \text{ht}\,, \\
g_{B_s B_{1s} \gamma} &\approx -(0.69\, Q_s - 0.52\, Q_b)|_{\text{PT}} - 1.03\, Q_s|_{\text{twist-2}} + \text{ht}\,,
\end{aligned} \tag{3.22}$$

where Q_i are the standard quark charges $Q_b = Q_d = Q_s = -\frac{1}{3}$ and $Q_c = Q_u = \frac{2}{3}$ and "ht" stands for higher twist and $q = u, d$. The size of the higher twist can be inferred from table 3. The twist-3 contribution is up to 5% in some cases and, as previously argued, most twist-4 contributions have to be dropped since they are incomplete without the inclusion of 4-particle DAs (cf. section 3.5.1 for further relevant remarks in this direction).

We now proceed to discuss the numerical features of the B- and D-meson results in turn. Beginning with the *B-mesons*, for the values given in table 2 we find that the daughter SRs (3.20) are, in all cases, satisfied to within $\lesssim 2\%$. The continuum contributions range from $\lesssim 25\%$ in the $\perp$-modes to $\lesssim 35\%$ in the $\parallel$-modes. In the $\perp$-modes the SR is dominated by the perturbative and twist-2 contributions which are approximately equal in size and are of the same sign. The remaining contributions make up $\approx$ 10–20% of the total. The story is repeated in the tensor $\parallel$-modes, however the situation in the vector $\parallel$-modes is somewhat altered. Here unfortunate cancellations act to suppress the perturbative contribution and the twist-2 sector is numerically dominant providing $\mathcal{O}(80)\%$ of the total value. A breakdown of contributions according to twist is given in table 3 for a representative selection of residues. The $\mathcal{O}(\alpha_s)$ corrections are mass scheme dependent. In the kinetic mass scheme ($\mu_{\text{kin}} = 1\,\text{GeV}$) employed the NLO results are sizeable, providing a correction of $\approx$ 20–35% and $\approx$ 20–25% at twist-1 and -2, respectively cf. table 3. The benefit and necessity of an NLO computation is clearly visible in the scale variation plots shown in figure 2 as residual effects are then of $\mathcal{O}(\alpha_s^2)$.

The SR parameters for the *D-mesons* are determined subject to the same tests as outlined above. In all cases the continuum contribution remains below 30% and in the

JHEP09(2021)023

twist	pa	DA	$r_\perp^V(B_u)$	$r_\parallel^V(B_d)$	$r_\perp^T(B_s)$	$r_\parallel^T(B_d)$	$r_\perp^V(D_u)$	$r_\perp^V(D_d)$	$r_\perp^T(D_d)$
1	–	PT: $\mathcal{O}(\alpha_s^0)$	-0.116	-0.014	0.102	0.033	-0.177	0.004	0.014
1	–	PT: $\mathcal{O}(\alpha_s)$	-0.033	0.003	0.027	-0.005	-0.047	-0.002	$< 10^{-3}$
2	2	$\phi_\gamma(u)\,\mathcal{O}(\alpha_s^0)$	-0.136	0.075	0.063	0.064	-0.220	0.110	0.078
2	2	$\phi_\gamma(u)\,\mathcal{O}(\alpha_s)$	-0.028	0.015	0.015	0.015	-0.028	0.014	0.018
3	2	$\Psi_{(a)}(u)$	0.011	–	0.016	-0.001	0.021	-0.010	-0.010
3	2	$\Psi_{(v)}^{(1)}(u)$	–	$< 10^{-3}$	0.001	$< 10^{-3}$	–	–	0.005
3	3	$\mathcal{A}(\underline{\alpha})$	–	–	$< 10^{-3}$	$< 10^{-3}$	–	–	-0.001
3	3	$\mathcal{V}(\underline{\alpha})$	–	–	-0.002	-0.003	–	–	-0.014
4	2	$h_\gamma^{(2)}(u)$	–	-0.003	$< 10^{-3}$	-0.002	–	–	-0.003
4	2	$\mathbb{A}(u)$	0.017	-0.05	-0.003	-0.003	0.033	-0.017	-0.006
4	3	$S(\underline{\alpha})+\tilde{S}(\underline{\alpha})$	$< 10^{-3}$	$< 10^{-3}$	$< 10^{-3}$	$< 10^{-3}$	-0.003	0.001	0.002
4	3	$\sum_{i=1}^{4} T_i^{(1)}(\underline{\alpha})$	-0.001	$< 10^{-3}$	$< 10^{-3}$	$< 10^{-3}$	-0.007	0.003	$< 10^{-3}$
4	3	$S_\gamma(\underline{\alpha})$	-0.008	$< 10^{-3}$	0.003	0.003	-0.033	-0.033	-0.026
4	3	$T_4^\gamma(\underline{\alpha})$	0.002	$< 10^{-3}$	$< 10^{-3}$	$< 10^{-3}$	0.007	0.007	$< 10^{-3}$
4	–	$Q_q\,\langle\bar{q}q\rangle$	–	0.002	–	–	–	–	–
4	–	$Q_b\,\langle\bar{q}q\rangle$	0.003	-0.002	0.002	0.002	-0.021	-0.021	-0.017
		Total*	-0.290	0.070	0.223	0.102	-0.475	0.096	0.081

Table 3. A breakdown of contributions according to twist, "pa" = number of partons and the specific DA. The definitions of the DAs can be found in [3]. The asterisk in total is a reminder that it does not include twist-4 contributions not closing under the equations of motion cf. [3].

neutral modes the daughter SR (3.20) is satisfied to within 3%. In the charged mode the daughter SR shows poor convergence. Again, this is due to the presumably artificial smallness of the perturbative contribution due to cancellation in Q_c and Q_u (cf. table 3 and (3.22)). In contrast to the B-mesons we note that whilst the dominant contribution arises from the twist-1 or -2 sectors the twist-3 and -4 sectors are sizeable, in particular in the charged case. The $\mathcal{O}(\alpha_s)$ corrections to twist-2 range from $\approx 12\%$ of the LO result in the vector modes to $\approx 20\%$ in the tensor modes. In the twist-1 sector the tensor modes and the neutral vector mode have radiative corrections ranging between ≈ 2–30%. In the charged vector modes, however, the corrections are $> 50\%$, due to the previously mentioned large charge cancellation at LO.

The uncertainty due to the input parameters is estimated by varying each parameter, within the given interval, in turn and adding each individual uncertainty in quadrature. A breakdown of the individual uncertainties is given in table 4. To incorporate correlations between the various thresholds, discussed previously, we generate 300 samples of the thresholds according to a Gaussian distribution such that the mean corresponds to

JHEP09(2021)023

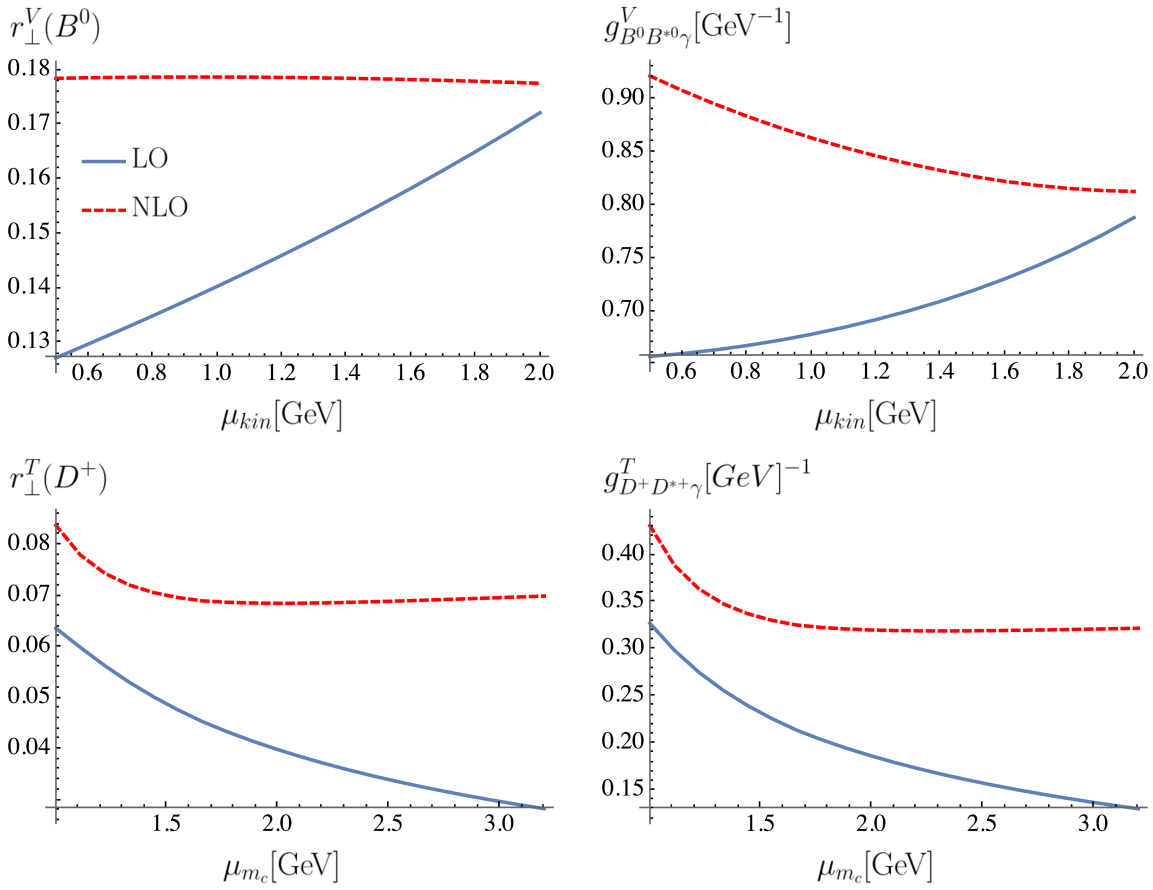

Figure 2. Representative plots highlighting how the NLO result (dashed red) sees a reduction in the mass scheme scale $\mu_{\rm kin}(\mu_{\overline{\rm MS}})$ as compared to LO (solid blue). We note that in the B-meson case the residue generally shows greater stability than the coupling which, in the above cases, inherits the (artificial) scale dependence of f_{B^*} which is less pronounced for f_{D^*} as the plots show.

the central value of each threshold and the standard deviation reproduces the associated uncertainty. We then evaluate the desired quantity for each of these samples, taking the standard deviation of the resulting points to be the uncertainty due to threshold variation. Our predictions for the couplings are given as the mean value of the vector and tensor interpolating current determinations. We estimate the associated uncertainty as the standard deviation of the two evaluations. Moreover, the uncertainty associated with varying the duality window is taken to be the standard deviation of the $a = \{1/2, 1, 2\}$ determinations (cf. table 5). This provides a small contribution in the B-meson cases, but notably a more significant contribution in the D_s mode. Adding in quadrature the uncertainty from all sources, we obtain the total uncertainty as quoted in table 7.

The final values for the residues and the couplings are shown in tables 6 and 7 respectively. The value of the coupling presented in the table is the average of the vector and tensor determinations.

JHEP09(2021)023

	$r_\perp^V(B_u)$	$r_\parallel^V(B_d)$	$r_\perp^T(B_s)$	$r_\parallel^T(B_d)$	$r_\perp^V(D_u)$	$r_\perp^V(D_d)$	$r_\perp^T(D_d)$
Value	-0.300	0.076	0.224	0.104	-0.473	0.095	0.073
Error	$^{+0.034}_{-0.033}$	$^{+0.015}_{-0.016}$	$^{+0.023}_{-0.024}$	$^{+0.015}_{-0.015}$	$^{+0.054}_{-0.053}$	$^{+0.021}_{-0.021}$	$^{+0.020}_{-0.020}$
$\Delta\overline{s_0}$	±0.021	±0.007	±0.017	±0.007	±0.033	±0.004	±0.004
$\Delta\hat{M}^2$	$^{+0.005}_{-0.000}$	$^{+0.001}_{-0.002}$	$^{+0.000}_{-0.002}$	$^{+0.000}_{-0.002}$	$^{+0.004}_{-0.001}$	$^{+0.001}_{-0.002}$	$^{+0.004}_{-0.001}$
$\Delta M_{f_B}^2$	$^{+0.000}_{-0.003}$	$^{+0.001}_{-0.000}$	$^{+0.004}_{-0.000}$	$^{+0.001}_{-0.000}$	$^{+0.000}_{-0.004}$	$^{+0.001}_{-0.000}$	$^{+0.001}_{-0.000}$
$\Delta m_{b,c}$	±0.002	±0.004	±0.002	±0.002	±0.003	±0.003	±0.003
$\Delta\tau$	±0.010	±0.006	±0.005	±0.005	±0.015	±0.008	±0.006
$\Delta\langle\bar{q}q\rangle$	±0.003	±0.001	±0.001	±0.001	±0.005	±0.004	±0.003
Δa_2	±0.020	±0.011	±0.009	±0.010	±0.033	±0.016	±0.012
$\Delta_{t=3}$	±0.006	$< 10^{-3}$	±0.004	±0.003	±0.011	±0.006	±0.011
$\Delta\mu_{\text{kin}}$	±0.003	±0.003	±0.002	±0.004	–	–	–
$\Delta\mu_m$	–	–	–	–	$^{+0.008}_{-0.001}$	$^{+0.004}_{-0.006}$	$^{+0.004}_{-0.007}$
$\Delta\mu_{\alpha_s}$	$^{+0.010}_{-0.003}$	$^{+0.001}_{-0.004}$	$^{+0.001}_{-0.003}$	$^{+0.001}_{-0.001}$	$^{+0.002}_{-0.003}$	$< 10^{-3}$	$^{+0.002}_{-0.001}$
$\Delta\mu_F$	$^{+0.002}_{-0.000}$	$^{+0.001}_{-0.004}$	$^{+0.002}_{-0.007}$	$^{+0.000}_{-0.001}$	$^{+0.005}_{-0.002}$	$^{+0.004}_{-0.001}$	$^{+0.000}_{-0.001}$
$\Delta\mu_{\text{UV}}$	–	–	±0.002	±0.001	–	–	±0.001
$\Delta\frac{\langle\bar{q}q\rangle}{\langle\bar{s}s\rangle}$	–	–	±0.002	–	–	–	–
$\Delta\Sigma$	±0.001	±0.003	±0.006	±0.006	±0.013	±0.002	±0.006

Table 4. Breakdown of the main contributions to the uncertainty for a representative selection of residues. $\Delta\overline{s_0}$ includes the combined uncertainty, incorporating correlations, due varying all effective thresholds, cf. discussion above (3.1). $\Delta_{t=3}$ contains the total uncertainty due to all twist-3 hadronic parameters $\{f_{3\gamma}, \omega_\gamma^A, \omega_\gamma^V\}$. The uncertainty due to the choice of duality region is encapsulated in the quantity $\Delta\Sigma$ which represents the standard deviation of the $a = \{1/2, 1, 2\}$ evaluations. The total uncertainty, which also includes smaller contributions such as the gluon condensate, is obtained by added uncertainties in quadrature.

	$g_{B_dB_d^*\gamma}$	$g_{B_sB_s^*\gamma}$	$g_{B_uB_u^*\gamma}$	$g_{B_dB_{1d}\gamma}$	$g_{B_sB_{1s}\gamma}$	$g_{B_uB_{1u}\gamma}$	$g_{D_dD_d^*\gamma}$	$g_{D_sD_s^*\gamma}$	$g_{D_uD_u^*\gamma}$
$a = 1/2$	0.86	0.96	−1.43	0.35	0.42	−0.70	0.38	0.69	−2.03
$a = 1$	0.86	0.95	−1.44	0.37	0.44	−0.72	0.40	0.60	−2.11
$a = 2$	0.86	0.94	−1.43	0.40	0.48	−0.74	0.40	0.52	−2.03

Table 5. Values of the coupling for different values of the duality parameter a (cf. section 3.4.1 and (3.17)). The majority of couplings show little dependence on the duality parameter a. Notable exceptions are the neutral B_1-couplings and the charged D^*-couplings. This does not come as a surprise as precisely those are plagued by, unfortunate, cancellations in the perturbative contribution of the $Q_{b,c}$- and Q_q-parts (cf. end of section 3.5.1 for comments).

JHEP09(2021)023

		$r_\perp^V$	$r_\perp^T$	$r_\parallel^V$	$r_\parallel^T$
$\mu_{\rm kin} = 1.0\,{\rm GeV}$	B_d	$0.179^{+0.019}_{-0.019}$	$0.171^{+0.018}_{-0.020}$	$0.076^{+0.015}_{-0.016}$	$0.104^{+0.015}_{-0.015}$
	B_s	$0.235^{+0.024}_{-0.025}$	$0.224^{+0.023}_{-0.024}$	$0.114^{+0.016}_{-0.018}$	$0.146^{+0.017}_{-0.017}$
	B_u	$-0.300^{+0.034}_{-0.033}$	$-0.284^{+0.033}_{-0.031}$	$-0.159^{+0.031}_{-0.029}$	$-0.199^{+0.028}_{-0.028}$
$\mu_{\overline{\rm MS}} = m_c(m_c)$	D_d	$0.095^{+0.021}_{-0.021}$	$0.073^{+0.020}_{-0.020}$	–	–
	D_s	$0.172^{+0.033}_{-0.029}$	$0.140^{+0.048}_{-0.046}$	–	–
	D_u	$-0.473^{+0.054}_{-0.053}$	$-0.412^{+0.049}_{-0.049}$	–	–

Table 6. The residues (2.5), related to form factors, for the B- and D-mesons. The former are determined in the kinetic scheme and the latter in the $\overline{\rm MS}$ scheme.

3.5.1 Comparison with literature and experiment

It is of interest to compare to the existing literature and experiment. The values of the couplings obtained in this work, which constitute the mean value of the tensor and vector determinations, along with determinations from other computations as well as experiment are collected in table 7. Unfortunately only two of the six couplings can be inferred from experiment as the widths of the vector mesons are too often unknown.[11] Moreover, in this section we use $(B_u, B_d, D_d, D_u) \to (B^+, B^0, D^+, D^0)$ which is the notation often used in experiment.

With regards to the two experimental values, we update the analysis in [11] and make some further comments. We first turn to the D^{*+}, for which the width $\Gamma(D^{*+}) = 83.4(18)\,{\rm keV}$ and branching fraction $B(D^{*+} \to D^+\gamma) = 0.016(4)$ are known [31], and with (2.2) give $|g_{D^+D^{*+}\gamma}| = 0.47(7)\,{\rm GeV}^{-1}$ instead of the previous $0.50(8)\,{\rm GeV}^{-1}$ in [11]. For D^{*0} the width is unknown and one needs to rely on isospin to infer it [11]. First we deduce g_c, related to the $D^{*+}D\pi$-coupling, as $g_c = 0.57(7)$, which is down from 0.61(7) in [11]. Considering all decay channels one then obtains $\Gamma(D^{*0}) = 56.5(14.0)\,{\rm keV}$, down from $68(17)\,{\rm keV}$ in [11]. Using the branching fraction $B(D^{*0} \to D^0\gamma) = 0.353(9)\,{\rm keV}$, down from $0.381(29)\,{\rm keV}$ we get $|g_{D^0D^{*0}\gamma}| = 1.77(16)\,{\rm GeV}^{-1}$, down from $2.02(26)\,{\rm GeV}^{-1}$ in [11].

Our result $g_{D^0D^{*0}\gamma} = 2.11^{+0.35}_{-0.34}\,{\rm GeV}^{-1}$ is compatible with experiment and so are the results of the other method. Our value for $g_{D^+D^{*+}\gamma} = 0.40^{+0.12}_{-0.13}\,{\rm GeV}^{-1}$ is again compatible with the new experimental value $|g_{D^+D^{*+}\gamma}| = 0.47(7)\,{\rm GeV}^{-1}$. Differences between this work and the LCSR computation [10] are noticeable and can be at least partially accounted for by computational differences. Firstly, we have computed twist-1 $\mathcal{O}(\alpha_s)$-corrections whereas they did not. Secondly, we include linear quark mass correction at LO and in the magnetic vacuum susceptibility χ_q (cf. section 3.2.1 in [3]). Third and most importantly, we drop twist-4 corrections other than the $Q_b\langle\bar{q}q\rangle$ condensate cf. previous section. For the B-meson case the twist-4 corrections are not large and the impact is small and the differences can be attributed to the first two cases. For the D-mesons higher twist corrections are

[11] The situation is different to the $g_{BB^*\pi}$ couplings as there the $B^* \to B\pi$ decay is kinematically forbidden and thus it seems unfortunate that the $B^*(B_1) \to B\gamma$ transitions are not known because of unknown total widths.

JHEP09(2021)023

units [GeV^{-1}]	$g_{B^0B^{*0}\gamma}$	$g_{B_sB_s^*\gamma}$	$g_{B^+B^{*+}\gamma}$	$g_{D^+D^{*+}\gamma}$	$g_{D_sD_s^*\gamma}$	$g_{D^0D^{*0}\gamma}$
This work	$0.86^{+0.15}_{-0.15}$	$0.95^{+0.15}_{-0.16}$	$-1.44^{+0.27}_{-0.26}$	$0.40^{+0.12}_{-0.13}$	$0.60^{+0.19}_{-0.18}$	$-2.11^{+0.35}_{-0.34}$
LCSR (NLL) [10]	$-0.91^{+0.12}_{-0.13}$	$-0.74^{+0.09}_{-0.10}$	$1.44^{+0.22}_{-0.20}$	$-0.15^{+0.11}_{-0.10}$	$-0.079^{+0.086}_{-0.078}$	$1.48^{+0.29}_{-0.27}$
HHχPT [18]	$-1.01^{+0.05}_{-0.05}$	$-0.70^{+0.06}_{-0.06}$	$1.45^{+0.11}_{-0.11}$	$-0.27^{+0.05}_{-0.05}$	$0.041^{+0.056}_{-0.056}$	$2.19^{+0.11}_{-0.11}$
VMD + HQET [28]	$-0.58^{+0.12}_{-0.10}$	–	$0.99^{+0.19}_{-0.13}$	$-0.29^{+0.19}_{-0.11}$	$-0.19^{+0.19}_{-0.08}$	$1.60^{+0.35}_{-0.45}$
CQM + HQET [29]	$-0.82^{+0.06}_{-0.05}$	–	$1.45^{+0.11}_{-0.12}$	$-0.38^{+0.05}_{-0.04}$	–	$1.91^{+0.09}_{-0.09}$
RQM [30]	$-0.93^{+0.05}_{-0.05}$	$0.65^{+0.03}_{-0.03}$	$1.66^{+0.11}_{-0.11}$	$-0.44^{+0.06}_{-0.06}$	$-0.19^{+0.03}_{-0.03}$	$2.15^{+0.11}_{-0.11}$
Lattice [11]*, [12]‡	–	–	–	$-0.20^{+0.30}_{-0.30}$*	$0.11^{+0.02}_{-0.02}$‡	$2.00^{+0.60}_{-0.60}$*
Experiment [31]	–	–	–	$0.47^{+0.07}_{-0.07}$	–	$1.77^{+0.16}_{-0.16}$†
units [GeV^{-1}]	$g_{B^0B_1^0\gamma}$	$g_{B_sB_{1s}\gamma}$	$g_{B^+B_1^+\gamma}$			
This work	$0.37^{+0.12}_{-0.12}$	$0.44^{+0.12}_{-0.12}$	$-0.72^{+0.21}_{-0.20}$			

Table 7. †The experimental value of $g_{D^0D^{*0}\gamma}$ requires the use of isospin symmetry to deduce the width of the D^{*0} cf. the main text in section 3.5.1. Here we take $(B_u, B_d, D_d, D_u) \to (B^+, B^0, D^+, D^0)$ to conform to PDG. Note that the sign cannot be determined from experiment and that for the theory results it is convention dependent cf. (A.3). We further note that $g_{B_sB_s^*\gamma} = \frac{f_{B_s}}{f_{B_s^*}}\frac{m_{B_s^*}}{m_{B_s}}|\mu| \approx 1.18\,\mathrm{GeV}^{-1}$ with $|\mu| = 1.13\,\mathrm{GeV}^{-1}$ from [32], deduced from D^*-decays and subject to $1/m_c$ corrections, is rather close to our value given the difference in methods. Whereas ref. [9] established that the D-couplings can be determined from LCSR we do not include the LO results presented therein as the input is outdated and a numerical comparison seems of limited use.

more important per se, as they are less convergent. In addition, for the charged case perturbation theory is presumably artificially suppressed which makes these results less reliable in general. Another important aspect is that in the charged case the inclusion of S_γ and $T_{4\gamma}$ is definitely incomplete as the photon can connect to the external states. A sign of this is that in the neutral case the twist-4 contributions cancel, whereas in the charged case they are additive cf. table 3.

The lattice determination $g_{D_sD_s^*\gamma}|_{[12]} = 0.11(2)$ is approximately three standard deviations lower than our value $g_{D_sD_s^*\gamma} = 0.60(19)$. This is where the breakdown (3.22) is useful. We find $g_{D_sD_s^*\gamma} \approx -0.6\,Q_c - 3.0\,Q_s$ and from figure 3 in [12] one deduces $g_{D_sD_s^*\gamma}|_{[12]} \approx -0.66Q_c - 1.65Q_s$. Whilst it is noted that in both cases the charm and strange quark contribution largely cancel each other, the effect is more pronounced for the lattice result. The charm contribution is rather close and the deviation is in the strange quark part with almost a factor 2 difference, which seems large but not as large as the initial number would suggest. It is instructive to investigate the $D^{*+} \to D^+\gamma$ case as by D-spin symmetry,[12] one would roughly expect a 20–30%-deviation. For our computation this is indeed the case $g_{D^+D^{*+}\gamma} \approx -0.65\,Q_c - 2.5\,Q_d \approx 0.40(13)$, which does agree reasonably well with experiment $g_{D^+D^{*+}\gamma} = 0.47(7)$ (cf. table 7). Concerning the question of D-spin breaking, some further guidance can be obtained from the lattice evaluation of the $D_{d,s} \to \gamma$

[12]The exchange of $d \leftrightarrow s$, which is still a good approximate symmetry under QED.

JHEP09(2021)023

form factors [33]. The fits to a linear and an extended pole model are in agreement with 20–30% D-spin breaking close to the kinematic endpoint. If the same level of D-spin breaking were valid at the $m^2_{D^*}$-pole, which some past experience suggests, then $g_{D^+D^{+*}\gamma}$ and $g_{D_sD_s^*\gamma}$ should not deviate considerably more than 20–30% from each other. If the former is true then this gives rise to a tension between the experimental $g_{D^+D^{+*}\gamma} = 0.47(7)$ and the lattice determination of $g_{D_sD_s^*\gamma}|_{[12]} = 0.11(2)$. In conclusion it remains somewhat unclear what the resolution of this puzzle is. Whereas the sum rule results seems consistent, we wish to emphasise that, in exactly these modes, the sum rules are not the best of their kind for various reasons. It may well be that the level of cancellations between the strange and the charm charge contributions are so severe that past experience is overthrown. It would be helpful to have further lattice determinations of these couplings and in particular a more precise one for $g_{D^+D^{+*}\gamma}$.

4 The $f_H, f_{H^*}, f_{H_1}, f^T_{H^*}$ and $f^T_{H_1}$ decay constants from QCD sum rules

The main reason for computing the decay constants is that to the best of our knowledge $\{f^T_{H^*}, f^T_{H_1}\}$, required for the relation between the couplings and the (form factor) residues (2.5), have not been subjected to a QCD SR evaluation and are thus new. The quantities f_B and f_{B^*} have previously been computed [13–15] to NLO with even partial NNLO results. We recompute these SRs and find agreement with the analytic expressions of the first two references.[13] In the work [15] the $\mathcal{O}(\alpha_s)\langle\bar{q}q\rangle$ corrections were computed independently and we do disagree with some the expression e.g. the incomplete Gamma function. Compare equation (21) [15] versus (B.6) and equation (59) in [14].

4.1 The computation

The starting points for the computations are the "diagonal" correlation functions

$$\begin{aligned}
\Gamma^{f_B}(p) &= i\int_x e^{ipx}\langle 0|T\{J_B(x)J_B^\dagger(0)\}|0\rangle &&= \Gamma_{f_B}(p^2)\,,\\
\Gamma^{f_{B^*}}_{\alpha\beta}(p) &= i\int_x e^{ipx}\langle 0|T\{J_\alpha(x)J_\beta^\dagger(0)\}|0\rangle &&= V_{\alpha\beta}\Gamma_{f_{B^*}}(p^2) + \tilde{V}_{\alpha\beta}\tilde{\Gamma}_{f_{B^*}}(p^2)\,,\\
\Gamma^{f^T_{B^*}}_{\alpha\beta\gamma\delta}(p) &= i\int_x e^{ipx}\langle 0|T\{J^T_{\alpha\beta}(x)J^{T\dagger}_{\gamma\delta}(0)\}|0\rangle &&= T_{[\alpha\beta][\gamma\delta]}\Gamma_{f^T_{B^*}}(p^2) + \tilde{T}_{\alpha\beta\gamma\delta}\tilde{\Gamma}_{f^T_{B^*}}(p^2)\,,
\end{aligned}$$

where we have taken $H = B$ for concreteness again. Above $J_\alpha = \bar{q}\gamma_\alpha b$, $J^T_{\alpha\beta} = \bar{q}\sigma_{\alpha\beta}b$ and the previously encountered J_B is given in (3.2). The Lorentz structures are

$$V_{\alpha\beta} = \frac{p_\alpha p_\beta}{p^2} - g_{\alpha\beta}\,,\quad \tilde{V}_{\alpha\beta} = p_\alpha p_\beta\,,\quad T_{\alpha\beta\gamma\delta} = -g_{\alpha\gamma}\frac{p_\gamma p_\delta}{p^2}\,,\quad \tilde{T}_{\alpha\beta\gamma\delta} = \varepsilon_{\alpha\beta}{}^{\bar{\alpha}\bar{\beta}}\,\varepsilon_{\gamma\delta}{}^{\bar{\gamma}\bar{\delta}}T_{\bar{\alpha}\bar{\beta}\bar{\gamma}\bar{\delta}}\,.$$

The Lorentz invariant functions are related to the hadronic quantities as follows

$$\Gamma_{f_B} = \frac{m_B^4 f_B^2}{m_B^2 - p^2} + \dots\,,\quad \Gamma_{f_{B^*}} = \frac{m^2_{B^*} f^2_{B^*}}{m^2_{B^*} - p^2} + \dots\,,\quad \Gamma_{f^T_{B^*}} = \frac{m^2_{B^*}(f^T_{B^*})^2}{m^2_{B^*} - p^2} + \dots\,, \tag{4.1}$$

[13] A direct comparison with [13, 14] can be made by taking the limit $s_0 \to \infty$ in the results in appendix B, as we provide the correlation functions after taking the Borel transform with continuum subtraction.

JHEP09(2021)023

and the remaining structure $\tilde{\Gamma}_{f_{B^*}}(p^2)$ is related to $\Gamma_{f_B}(p^2)$ up to contact terms by the equation of motion. The correlation functions for the $\{f_{B_1}, f^T_{B_1}\}$ decay constants follow with rules for the insertion of the γ_5 into the currents cf. (B.10) and $B^* \to B_1$ in (4.1) following the ideas in [34].

The generic SR is parametrised by

$$f^2_{B_{(i)}} = \frac{e^{\frac{m^2_{B_{(i)}}}{M^2_{f_{B_{(i)}}}}}}{\omega_{B_{(i)}}} \left(\int_{m_b^2}^{s_0^{f_{B_{(i)}}}} ds\, e^{-\frac{s}{M^2_{f_{B_{(i)}}}}} \rho_{f_{B_{(i)}}}(s) + e^{\frac{-m_b^2}{M^2_{f_{B_{(i)}}}}} \left[c^{f_{B_{(i)}}}_{\langle\bar{q}q\rangle} m_b \langle\bar{q}q\rangle + c^{f_{B_{(i)}}}_{\langle G^2\rangle} \left\langle G^2 \right\rangle + \frac{m_b}{M^2_{f_{B_{(i)}}}} c^{f_{B_{(i)}}}_{\langle\bar{q}Gq\rangle} \langle\bar{q}Gq\rangle \right] \right), \tag{4.2}$$

where $f_{B_{(i)}}$ stands for any $\{f_B, f_{B^*}, f^T_{B^*}, f_{B_1}, f^T_{B_1}\}$, $\omega_B = m_B^4/(m_b+m_q)^2$ and $\omega_{B_{(i)}} = m^2_{B_{(i)}}$ otherwise. The local OPE is performed up to dim ≤ 5 including $\mathcal{O}(\alpha_s)$ corrections to both the perturbative and quark condensate contributions. Four quark condensates ($d = 6$) give contributions at the sub per mille level and are omitted. We have checked that all the scale dependences, due to NLO computations, are correct. This includes the cancellation of the condensate scale, denoted by μ_{cond}, up to $\mathcal{O}(\alpha_s^2)$ as well as the anomalous scaling of the scalar and transverse decay constants (2.7). Explicit results are given in appendix B.

The PDG value, for which the CKM matrix elements $|V_{\text{cd(s)}}|$ are inputs, deviates close to three standard deviations from the lattice result.

4.2 Numerical analysis

The numerical analysis is the same as for the residues/couplings except that the scales are taken to be different as, in contrast, there is no motivation to cancel terms in ratios. Concretely, the condensate and α_s scale are changed as shown, to the right of the vertical double separation, in table 1. This enforces a change in SR parameters $\{M^2_{f_B}, s_0^{f_B}\}$ according to the previous criteria, with thresholds fixed such that the daughter SR

$$m^2_{B_{(i)}} = M^4_{f_{B_{(i)}}} \frac{d}{dM^2_{f_{B_{(i)}}}} \ln \int_{m_b^2}^{s_0^{f_{B_{(i)}}}} ds\, e^{\frac{-s}{M^2_{f_{B_{(i)}}}}} \rho_{f_{B_{(i)}}}(s)\,, \tag{4.3}$$

reproduces the known value of the associated meson mass to $\approx 0.5\%$. The continuum contribution is kept below $\approx 45\%$. The SR parameters are given alongside the main results in table 8 (cf. table 12 for $\overline{\text{MS}}$-evaluation of the B-meson decay constants) and a representative breakdown of the uncertainty is given in table 9. Isospin breaking effects impact at the sub per mille level e.g. [46] and are therefore not considered as they are superseded by the actual uncertainties. If considered, it would seem sensible to include QED effects as well, which would then necessitate the inclusion of the radiative mode in addition.

The uncertainties of the decay constants are around 10% and in agreement with lattice results of $\mathcal{O}$(1–4%)-uncertainty. Moreover, we quote other QCD SR determinations, [14]

JHEP09(2021)023

$f_{B_{(i)}}\backslash B_{(i)}$(MeV)	$B(5280)$	$B_s(5367)$	$B^*(5325)$	$B_s^*(5415)$	$B_1(5726)$	$B_{1s}(5829)$
lattice [17, 35]	190.0(1.3)	230.3(1.3)	186.4(7.1)	223.1(5.6)	–	–
experiment [31]	188(17)(18)	–	–	–	–	–
SR [14]	207^{+17}_{-9}	242^{+17}_{-12}	210^{+10}_{-12}	251^{+14}_{-16}	335^{+18}_{-18} [15]	348^{+18}_{-18} [15]
SR [36]	193.4(16.6)	232.5(21.0)	–	–	–	–
this work	192^{+20}_{-19}	225^{+21}_{-20}	209^{+23}_{-22}	245^{+24}_{-23}	247^{+31}_{-29}	305^{+27}_{-26}
$\delta_{\rm PT}$, $\delta_{\langle\bar{q}q\rangle}$	0.18, -0.03	0.20, -0.02	0.10, -0.08	0.13, -0.07	0.11, -0.09	0.14, -0.05
$s_0^{f_{B_{(i)}}}$, $M^2_{f_{B_{(i)}}}$	34.4, 5.7	35.6, 6.6	34.9, 6.2	36.2, 6.9	38.1, 5.7	40.9, 8.1
$f^T_{B_{(i)}}\backslash B_{(i)}$(MeV)			$B^*(5325)^T$	$B_s^*(5415)^T$	$B_1(5726)^T$	$B_{1s}(5829)^T$
this work			200^{+21}_{-20}	236^{+22}_{-21}	230^{+29}_{-28}	285^{+25}_{-24}
$\delta_{\rm PT}$, $\delta_{\langle\bar{q}q\rangle}$			0.11, -0.08	0.14, -0.06	0.11, -0.09	0.14, -0.05
$s_0^{f_{B_{(i)}}}$, $M^2_{f_{B_{(i)}}}$			34.9, 6.2	36.3, 7.4	38.1, 5.7	40.9, 8.6
$f^{(T)}_{D_{(i)}}\backslash D_{(i)}$(MeV)	$D(1865)$	$D_s(1968)$	$D^*(2007)$	$D_s^*(2112)$	$D^*(2007)^T$	$D_s^*(2112)^T$
lattice [17, 35]	209.0(2.4)	248.0(1.6)	223.5(8.7)	268.8(6.5)	–	–
experiment [31]	203.7(47)(6)	257.8(41)(1)	–	–	–	–
SR [14]	201^{+12}_{-13}	238^{+13}_{-23}	242^{+20}_{-12}	293^{+19}_{-14}	–	–
SR [36]	206.2(12.4)	245.3(20.2)	–	–	–	–
this work	190^{+15}_{-15}	226^{+17}_{-17}	227^{+18}_{-17}	279^{+19}_{-19}	202^{+16}_{-16}	256^{+16}_{-17}
$\delta_{\rm PT}$, $\delta_{\langle\bar{q}q\rangle}$	0.24, 0.02	0.28, 0.03	0.05, -0.15	0.11, -0.11	0.07, -0.14	0.14, -0.10
$s_0^{f_{B_{(i)}}}$, $M^2_{f_{B_{(i)}}}$	5.7, 1.9	6.3, 2.2	5.9, 2.0	6.8, 2.7	5.8, 2.2	6.9, 3.0

Table 8. QCD SR results for the decay constants, in units of MeV, with the exception of the Borel parameter and the threshold which are given in GeV^2-units. The kinetic ($\mu_{\rm kin} = 1\,\text{GeV}$) and $\overline{\rm MS}$ ($\mu_m = m_c(m_c)$) schemes are employed for the B- and D-meson case respectively. Input values are given in table 14. For the $B(D)$-meson SR a uniform uncertainty $\Delta s_0 = \pm 1.5\,\text{GeV}^2$ ($\Delta s_0 = \pm 0.5\,\text{GeV}^2$), $\Delta M^2 = \pm 1.5\,\text{GeV}^2$ ($\Delta M^2 = \pm 0.5\,\text{GeV}^2$) is applied to the threshold and the Borel parameter. The slightly smaller uncertainty assigned to the decay constant SR parameters versus those of the residues reflects the fact that the daughter SR is satisfied to within $\approx 0.5\%$ in the former but only to within $\approx 2\%$ in the latter. The relative size of the radiative corrections are denoted by δX such that $f_{B_{(i)}}|_{X_{\rm NLO}} = f_{B_{(i)}}|_{X_{\rm LO}}(1+\delta_X)$, with $X = \{\text{PT}, \langle\bar{q}q\rangle\}$. For comparison we include the most recent lattice determinations. The $J^P = 0^-$ decay constants are taken from [35] which averages over values in [37–40] and [41–45] for the B- and D-mesons, respectively. For the $J^P = 1^-$ states we quote the values obtained in [17]. The experimental values are from the PDG review and the extraction of the decay constants involve the CKM matrix $|V_{\rm ub}|$ and $|V_{\rm cd(s)}|$ as inputs. The PDG-error is from the experiment and the CKM input in the first and second parentheses respectively. Note that the central values for f_{B_1} and $f_{B_{1s}}$ from [15] deviate considerably from ours which might be due to discrepancies in the $\mathcal{O}(\alpha_s)\langle\bar{q}q\rangle$-corrections (cf. remarks at the end of the first paragraph in section 4).

JHEP09(2021)023

	f_B	f_{B_s}	f_{B^*}	$f^T_{B^*}$	f_D	f_{D_s}	f_{D^*}	$f^T_{D^*}$
Value	192.3	224.8	209.0	199.7	189.6	225.7	226.7	202.1
Error	$^{+19.7}_{-18.6}$	$^{+21.3}_{-20.3}$	$^{+22.6}_{-21.2}$	$^{+20.7}_{-19.5}$	$^{+14.7}_{-15.4}$	$^{+17.1}_{-17.4}$	$^{+18.3}_{-16.5}$	$^{+16.0}_{-16.3}$
$\Delta s_0^{f_B}$	$^{+11.0}_{-9.5}$	$^{+12.3}_{-10.8}$	$^{+12.0}_{-10.4}$	$^{+10.7}_{-9.2}$	$^{+10.5}_{-8.9}$	$^{+10.8}_{-9.2}$	$^{+13.1}_{-11.1}$	$^{+11.6}_{-9.9}$
$\Delta M^2_{f_B}$	$^{+0.0}_{-1.8}$	$^{+0.0}_{-2.0}$	$^{+0.0}_{-1.0}$	$^{+0.0}_{-0.5}$	$^{+0.0}_{-1.7}$	$^{+0.0}_{-1.6}$	$^{+0.6}_{-0.2}$	$^{+0.8}_{-0.0}$
Δm_h	$^{+11.4}_{-11.7}$	$^{+11.8}_{-12.0}$	$^{+14.1}_{-14.6}$	$^{+12.9}_{-13.4}$	$^{+2.0}_{-1.9}$	$^{+2.0}_{-1.8}$	± 6.1	± 4.4
$\Delta\langle\bar{q}q\rangle$	± 1.7	± 1.4	± 1.7	± 1.8	± 2.7	± 2.2	± 3.0	± 2.8
$\Delta\mu_{\text{kin}}$	$^{+11.2}_{-10.1}$	$^{+11.9}_{-10.8}$	$^{+12.4}_{-10.5}$	$^{+11.2}_{-9.5}$	–	–	–	–
$\Delta\mu_m$	–	–	–	–	$^{+4.5}_{-10.2}$	$^{+4.4}_{-11.8}$	$^{+9.1}_{-8.1}$	$^{+6.6}_{-9.2}$
$\Delta\mu_{\alpha_s}$	$^{+1.8}_{-3.7}$	$^{+2.6}_{-5.2}$	$^{+1.0}_{-2.0}$	$^{+0.9}_{-1.8}$	$^{+7.5}_{-4.4}$	$^{+11.1}_{-6.4}$	$^{+0.7}_{-1.2}$	$^{+0.5}_{-0.9}$
$\Delta\mu_{\text{UV}}$	–	–	–	$^{+1.7}_{-2.0}$	–	–	–	$^{+3.2}_{-3.8}$
$\Delta\frac{\langle\bar{q}q\rangle}{\langle\bar{s}s\rangle}$	–	± 2.8	–	–	–	± 3.4	–	–
Δ_{hd}	± 1.0	± 0.5	± 3.1	± 3.7	± 3.8	± 3.2	± 5.4	± 5.8

Table 9. Breakdown of the main contributions to the uncertainty for a representative selection of decay constants in units of MeV in the kinetic scheme. The uncertainty Δ_{hd} covers higher dimensional condensates omitted from the OPE which are estimated as the values of the $d = 4, 5$ condensates. This is conservative as the four quark condensates are known to be a sub per mille effect. The total uncertainty also includes contributions not shown in the table, such as Δm_0^2 which has a negligible impact.

and [36]. We differ from these results mainly in two aspects. First we do not include partial NNLO effects but treat the mass scheme and the factorisation scale dependence μ_{cond} separately and thus more carefully. Secondly, we use a significant update of the strange quark condensate. We note that our values are also consistent with the classic Jamin and Lange result [13], $(f_B, f_{B_s}) = (210(19), 244(21))$ MeV.

4.2.1 Ratios of decay constants

Some of the decay constants are related by heavy quark and/or SU(3)$_F$ symmetries, and thus there is some tradition in investigating ratios and determining their deviation from unity. A total of 24 ratios are shown in table 10 (cf. table 13 for the $\overline{\text{MS}}$-evaluation of the B-meson ratios).

SU(3)$_F$-type ratios such as f_{B_s}/f_B are typically above 1 as one would intuitively expect. We quote our results, denoted by "PZ" for brevity instead of "this work", against some results from the literature

$$\left(\frac{f_{B_s}}{f_B}, \frac{f_{D_s}}{f_D}\right) = \begin{cases} (1.17(7), & 1.19(7) &) \text{ PZ SRs} \\ (1.209(5), & 1.174(7) &) \text{ [35] lattice} \\ (- & 1.265(36)) & \text{[31] experiment} \end{cases} . \tag{4.4}$$

Comparison with the lattice average and shows that there is good agreement albeit the precision in lattice QCD, at the sub per mille level, is beyond reach for QCD SRs. The

JHEP09(2021)023

f_{B_s}/f_B	$f_{B_s^*}/f_{B^*}$	$f_{B_{1_s}}/f_{B_1}$	$f^T_{B_s^*}/f^T_{B^*}$	$f^T_{B_{1_s}}/f^T_{B_1}$	f_{D_s}/f_D	$f_{D_s^*}/f_{D^*}$	$f^T_{D_s^*}/f^T_{D^*}$
1.17(7)	1.17(7)	1.23(8)	1.18(6)	1.24(8)	1.19(7)	1.23(8)	1.27(8)
f_{B^*}/f_B	f_{B_1}/f_B	f_{B_1}/f_{B^*}	$f^T_{B^*}/f_B$	$f^T_{B_1}/f_B$	$f^T_{B_1}/f^T_{B^*}$	f_{D^*}/f_D	$f^T_{D^*}/f_D$
1.09(6)	1.29(9)	1.18(9)	1.04(6)	1.20(9)	1.15(9)	1.20(11)	1.07(9)
$f_{B_s^*}/f_{B_s}$	$f_{B_{1_s}}/f_{B_s}$	$f_{B_{1_s}}/f_{B_s^*}$	$f^T_{B_s^*}/f_{B_s}$	$f^T_{B_{1_s}}/f_{B_s}$	$f^T_{B_{1_s}}/f^T_{B_s^*}$	$f_{D_s^*}/f_{D_s}$	$f^T_{D_s^*}/f_{D_s}$
1.09(6)	1.36(8)	1.24(8)	1.05(5)	1.27(8)	1.21(8)	1.23(9)	1.13(7)

Table 10. Ratios of various decay constants in the kinetic($\overline{\text{MS}}$) scheme for the $B(D)$-mesons. Comparison with the literature can be found in section 4.2.1. Ratios in the $\overline{\text{MS}}$ scheme for the B-mesons are given in table 13.

above lattice values are averaged over the works of [37, 39, 47, 48] and [42, 43, 45] for the B- and D-ratio respectively. The PDG value, for which the CKM matrix elements $|V_{\text{cd(s)}}|$ are inputs, deviates close to three standard deviations from the lattice result. Further ratios of interest stem from heavy quark symmetry which groups the B and the B^* meson into the same multiplet as in this (non-relativistic) limit the spin ceases to matter. Deviations of the rations from one therefore highlight sensitivities to effects beyond that limit and comparison with the literature

$$\left(\frac{f_{B^*}}{f_B},\frac{f_{B_s^*}}{f_{B_s}},\frac{f_{D^*}}{f_D},\frac{f_{D_s^*}}{f_{D_s}}\right)=\begin{cases}(1.09(6), & 1.09(6), & 1.20(11), & 1.23(9) &) \text{ PZ SRs}\\ (1.02^{+0.02}_{-0.09}, & 1.04^{+0.01}_{-0.08}, & 1.20^{+0.13}_{-0.07}, & 1.24^{+0.13}_{-0.05} &) \text{ [14] SRs}\\ (0.944(11)(18), & 0.947(23)(20), & - & - &) \text{ [49] SRs}\\ (- & - & - & 1.10(2) &) \text{ [12] lattice}\\ (1.051(17), & - & 1.208(27), & - &) \text{ [50] lattice}\\ (0.941(26), & 0.953(23), & - & - &) \text{ [51] lattice}\\ (0.958(22), & 0.974(10), & 1.078(36), & 1.087(20)) & \text{ [17] lattice}\end{cases}$$

does show some minor tension between the results. Note that the lattice result [50] is with $N_f = 2$ and [17, 51] are with $N_f = 2 + 1$ and thus more reliable. For further discussion of the possible reasons for discrepancies cf. section IV in [51].

We now proceed to give some detail on of the individual uncertainties of the ratios in the SR computation. In both the B- and D-meson rations the effective thresholds prove to be the largest source of uncertainty. Whilst correlations between the thresholds, discussed previously, act to constrain the error the contribution to the total uncertainty is still significant, sitting in the region of $\approx$ 70–80%. The remaining uncertainty can be mostly attributed to the associated quark mass and in the D-meson rations the coupling scale μ_{α_s} provides a contribution to the total uncertainty of a similar order. For the SU(3)$_F$-ratios in (4.4), the quark condensate ratio $\langle\bar{s}s\rangle/\langle\bar{q}q\rangle$ provides a notable contribution to the total uncertainty.

JHEP09(2021)023

$\Gamma(B^{*0}\to B^0\gamma)$ $0.16^{+0.06}_{-0.06}\,\text{keV}$	$\Gamma(B_s^*\to B_s\gamma)$ $0.24^{+0.08}_{-0.08}\,\text{keV}$	$\Gamma(B^{*+}\to B^+\gamma)$ $0.45^{+0.17}_{-0.16}\,\text{keV}$
$\Gamma(B_1^0\to B^0\gamma)$ $26.22^{+17.00}_{-17.00}\,\text{keV}$	$\Gamma(B_{1s}\to B_s\gamma)$ $41.14^{+22.44}_{-22.44}\,\text{keV}$	$\Gamma(B_1^+\to B^+\gamma)$ $99.30^{+57.92}_{-55.16}\,\text{keV}$
$\Gamma(D^{*0}\to D^0\gamma)$ $27.83^{+9.23}_{-9.50}\,\text{keV}$	$\Gamma(D_s^*\to D_s\gamma)$ $2.36^{+1.49}_{-1.41}\,\text{keV}$	$\Gamma(D^{*+}\to D^+\gamma)$ $0.96^{+0.58}_{-0.62}\,\text{keV}$

Table 11. Decay rates based on the g-couplings in table 7 and the decay rate formula (2.2).

5 Summary and discussion

In this work we have determined the couplings of photons to heavy-light quark mesons (2.3) from light-cone sum rules at next-to-leading order in α_s at the twist-1,-2 level, at leading order in twist-3, and partial twist-4.[14] We have also investigated the effect of various duality regions (cf. section 3.4.1 and table 5) and have found the impact to be small. Our main results, with uncertainties of $\mathcal{O}(15\%)$, are given in table 7 along other theoretical and experimental results for comparison. The residues related to the $\bar{B}\to\gamma$ form factors, as in (2.4) and (2.5), are given in table 6. As a by-product we have determined the heavy decay constants $f_H, f_{H^*}, f_{H_1}, f_{H^*}^T$ and $f_{H_1}^T$ $(H=B,D)$ in QCD sum rules at next-to-leading order.[15] To the best of our knowledge $\{f_{B^*(D^*)}^T, f_{B_1}^T\}$ have not been evaluated with QCD sum rules and we therefore close a gap in the literature. Agreement is found with existing results, where comparison is possible, on the analytic and numerical level cf. table 8. Our treatment differs, besides a significant update to the strange quark condensate, in that we treat the mass-scheme and the factorisation scale dependence μ_{cond} separately and thus more carefully, but do not include partial $\mathcal{O}(\alpha_s^2)$ corrections to perturbation theory. Ratios of decay constant are given in table 10 and compared to the literature in section 4.2.1. We now turn to phenomenological aspects. The coupling determinations lead to the radiative decay predictions given in table 11, consistent with the experimentally known D^+/D^0-rates. It's unfortunate that the B-rates are not experimentally known as our predictions are more reliable in that sector (e.g. independence of the interpolating current and convergence of the twist expansion). Particularly for the D^+/D_s-channels there is the additional issue of large cancelation of the Q_c- and $Q_{q/s}$-contributions which present a challenge for all theory approaches (cf. the discussion in section 3.5.1). An important aspect is the interplay with the real QED-corrections in leptonic decays $H\to\ell\bar{\nu}(\gamma)$. This is the case since the couplings describe the pole residue (2.4) and [52] which, bearing in mind previously mentioned cancellations, should play a significant role in the soft-photon emission. In view of the importance of QED-corrections at the precision frontier, these couplings will hopefully attract further attention from the experimental and theory community.

[14] We have argued (cf. section 3.3. in [3]) that most twist-4 parameters require the inclusion of 4-particle distribution amplitudes which have not been classified to date. This can be seen from the equation of motion for the form factors not closing or by writing down the 4-particle distribution amplitude of twist-4 and subjecting it to the equation of motion of distribution amplitudes.

[15] With the exception of the D_1 as it is not well isolated cf. footnote 1.

JHEP09(2021)023

Acknowledgments

RZ is supported by an STFC Consolidated Grant, ST/P0000630/1. BP is supported by an STFC Training Grant, ST/N504051/1. We are grateful to Marco Pappagallo, Christine Davies, Giuseppe Gagliardi, Christopher Sachrajda for useful discussions and to James Gratrex for thorough proofreading of the manuscript.

A Convention, definitions and additional tables

In this appendix we collect conventions, definitions and input parameters.

A.1 Convention and definitions

We use the convention $\varepsilon_{0123} = 1$ for the Levi-Civita tensor and $D_\mu = \partial_\mu + s_e ieQ_f A_\mu + s_g i g_s A_\mu$ for the covariant derivative ($e > 0$ and $Q_e = -1$ for the electron as a u-spinor). Below we will keep explicit factors s_i in place, which are assumed $s_i = 1$ throughout the main text, in order to facilitate comparison with the literature. The B_q-meson ($q = d, u, s$) decay constant is defined by

$$\langle 0|\bar{q}\gamma^\mu\gamma_5 b|\bar{B}_q(p_B)\rangle = s_B i p_B^\mu f_{B_q}\,, \tag{A.1}$$

and for the B_q^* (1^-) and B_{1q} (1^+) states via

$$\begin{aligned}
\langle 0|\bar{q}\,\gamma^\mu\, b|\bar{B}_q^*(p)\rangle &= s_{B^*} m_{B_q^*} f_{B_q^*}\eta^\mu\,, & \langle 0|\bar{q}\,\gamma^\mu\gamma_5\, b|\bar{B}_{1q}(p)\rangle &= m_{B_{1q}} s_{B_1} f_{B_{1q}}\eta^\mu\,,\\
\langle 0|\bar{q}\,\sigma^{\mu\nu}\, b|\bar{B}_q^*(p)\rangle &= i s_{B^*} f_{B_q^*}^T \eta^{[\mu}p^{\nu]}\,, & \langle 0|\bar{q}\,\sigma^{\mu\nu}\gamma_5\, b|\bar{B}_{1q}(p)\rangle &= -i s_{B_1} f_{B_{1q}}^T \eta^{[\mu}p^{\nu]}\,.
\end{aligned} \tag{A.2}$$

The definition for the $D-$, D^*- and D_1-mesons are analogous. With these conventions the couplings the effective Lagrangian (2.3) assumes the form

$$\mathcal{L}_{\text{eff}} = s_e s_B s_{B^*}\frac{1}{2} g_{BB^*\gamma}\,\epsilon(B^*, \partial B^\dagger, F) - i s_e s_B s_{B_1} g_{BB_1\gamma}\, B_{1\alpha}\partial_\beta B^\dagger F^{\alpha\beta} + \text{h.c.}\,. \tag{A.3}$$

For completeness we state the definition of the $B \to \gamma$ form factors used in [3]

$$\begin{aligned}
\langle\gamma(k,\epsilon)|O_\mu^V|\bar{B}_q(p_B)\rangle &= s_B s_e(P_\mu^\perp V_\perp(q^2) - P_\mu^\parallel\left(V_\parallel(q^2) + Q_{\bar{B}_q}\frac{2f_{B_q}/m_{B_q}}{1-q^2/m_{B_q}^2} + \dots\right),\\
\langle\gamma(k,\epsilon)|O_\mu^T|\bar{B}_q(p_B)\rangle &= s_B s_e(P_\mu^\perp T_\perp(q^2) - P_\mu^\parallel T_\parallel(q^2))\,,
\end{aligned} \tag{A.4}$$

where $P_\mu^\perp$ and $P_\mu^\parallel$ are defined in the main text (3.3), $Q_{\bar{B}_q}$ is the $\bar{B}$-meson charge and the dots represents the Low-term (or contact term) which is not important for this paper (cf. [3] for details). Note that, the point-like term, proportional to f_B, is not be included for the $g_{B_u B_{1u}\gamma}$ coupling as it is not associated with the B_{1u}-pole. The local operators in (A.4) are given by $O_\mu^{V[T]} \equiv O_{\perp\mu}^{V[T]} + O_{\parallel\mu}^{V[T]}$, with

$$\begin{aligned}
O_{\perp\mu}^V &\equiv -\frac{1}{e} m_{B_q}\bar{q}\gamma_\mu b\,, & O_{\perp\mu}^T &\equiv \frac{1}{e}\bar{q}iq^\nu\sigma_{\mu\nu}b\,,\\
O_{\parallel\mu}^V &\equiv \frac{1}{e} m_{B_q}\bar{q}\gamma_\mu\gamma_5 b\,, & O_{\parallel\mu}^T &\equiv \frac{1}{e}\bar{q}iq^\nu\sigma_{\mu\nu}\gamma_5 b\,.
\end{aligned} \tag{A.5}$$

JHEP09(2021)023

$H(\text{MeV})$	$B(5280)$	$B_s(5367)$	$B^*(5325)$	$B_s^*(5415)$	$B_1(5726)$	$B_{1s}(5829)$
$f_{B_{(i)}}$	213^{+22}_{-16}	248^{+23}_{-17}	218^{+23}_{-27}	260^{+23}_{-22}	288^{+25}_{-24}	341^{+20}_{-24}
δ_{PT}, $\delta_{\langle\bar{q}q\rangle}$	-0.03, -0.11	0.03, -0.06	-0.18, -0.23	-0.12, -0.22	-0.11, -0.19	-0.05, -0.13
$s_0^{f_{B_{(i)}}}$, $M^2_{f_{B_{(i)}}}$	33.6, 6.0	34.9, 7.2	33.7, 6.5	35.0, 6.8	39.0, 7.5	40.8, 9.4
$H(\text{MeV})$			$B^*(5325)^T$	$B_s^*(5415)^T$	$B_1(5726)^T$	$B_{1s}(5829)^T$
$f^T_{B_{(i)}}$			208^{+21}_{-23}	249^{+20}_{-19}	267^{+21}_{-22}	318^{+18}_{-22}
δ_{PT}, $\delta_{\langle\bar{q}q\rangle}$			-0.16, -0.24	-0.11, -0.24	-0.09, -0.19	-0.04, -0.14
$s_0^{f_{B_{(i)}}}$, $M^2_{f_{B_{(i)}}}$			33.7, 6.5	35.0, 6.8	39.0, 6.2	40.8, 9.4

Table 12. B-meson decay constants, MeV-units, determined in the $\overline{\text{MS}}$ scheme (kinetic scheme values in table 8)) with the Borel parameter and effective threshold given in GeV^2-units.

f_{B_s}/f_B $1.17^{+0.07}_{-0.07}$	$f_{B_s^*}/f_{B^*}$ $1.18^{+0.08}_{-0.08}$	$f_{B_{1s}}/f_{B_1}$ $1.18^{+0.08}_{-0.06}$	$f^T_{B_s^*}/f^T_{B^*}$ $1.19^{+0.07}_{-0.07}$	$f^T_{B_{1s}}/f^T_{B_1}$ $1.18^{+0.08}_{-0.05}$	
f_{B^*}/f_B $1.04^{+0.13}_{-0.08}$	f_{B_1}/f_B $1.35^{+0.12}_{-0.08}$	f_{B_1}/f_{B^*} $1.30^{+0.09}_{-0.10}$	$f^T_{B^*}/f_B$ $0.98^{+0.11}_{-0.07}$	$f^T_{B_1}/f_B$ $1.26^{+0.09}_{-0.07}$	$f^T_{B_1}/f^T_{B^*}$ $1.28^{+0.08}_{-0.10}$
$f_{B_s^*}/f_{B_s}$ $1.05^{+0.12}_{-0.07}$	$f_{B_{1s}}/f_{B_s}$ $1.37^{+0.09}_{-0.08}$	$f_{B_{1s}}/f_{B_s^*}$ $1.31^{+0.08}_{-0.11}$	$f^T_{B_s^*}/f_{B_s}$ $1.00^{+0.11}_{-0.07}$	$f^T_{B_{1s}}/f_{B_s}$ $1.28^{+0.08}_{-0.07}$	$f^T_{B_{1s}}/f^T_{B_s^*}$ $1.27^{+0.10}_{-0.08}$

Table 13. Ratios of decay constants in the $\overline{\text{MS}}$ scheme. The asymmetry of the uncertainty, most pronounced in the pseudo-scalar vs. vector vs. tensor channels, arises from an asymmetric variation of the $\overline{\text{MS}}$ scale, cf. table 1. The corresponding ratios in the kinetic scheme are given in table 10 which are compatible within uncertainties.

A.2 Additional tables

Here we provide some additional tables, namely the input parameters table 14, $\overline{\text{MS}}$ determinations of the decay constants table 12 and their ratios table 13.

We note that when fixing the SR parameters via the daughter SR we observe that the optimal value of the effective threshold for the B^* decay constant sits below that of the B. Clearly this does not make sense from a physical point of view and so we relax the condition on the daughter SR (4.3) such that it reproduces the associated meson mass to within 1.5%, which allows for the physical ordering of the thresholds to be imposed. We do not observe this problem when evaluating in the kinetic scheme which is another reason in its favour.

B Analytic results for the f_H, f_{H^*}, f_{H_1}, $f^T_{H^*}$ and $f^T_{H_1}$ decay constants

In this appendix we provide the analytic results for the decay constants $\{f_B, f_{B^*}, f_{B_1}, f^T_{B^*}, f^T_{B_1}\}$, with straightforward substitutions for the their D-meson counterparts. The

JHEP09(2021)023

Running coupling parameters

$\alpha_s(m_Z)$ [31]	m_Z [31]				
0.1176(20)	91.19 GeV				
$J^P = 0^-$ Meson masses [31]					
m_{B^0}	m_{B^+}	m_{B_s}	m_{D^0}	m_{D^+}	m_{D_s}
5.280 GeV	5.280 GeV	5.367 GeV	1.865 GeV	1.870 GeV	1.968 GeV
$J^P = 1^-$ Meson masses [31]					
$m_{B^{*0}}$	$m_{B^{*+}}$	$m_{B_s^*}$	$m_{D^{*0}}$	$m_{D^{*+}}$	$m_{D_s^*}$
5.325 GeV	5.325 GeV	5.415 GeV	2.007 GeV	2.010 GeV	2.112 GeV
$J^P = 1^+$ Meson masses [31]					
$m_{B_1^0}$	$m_{B_1^+}$	$m_{B_{1s}}$	$m_{D_1^0}$	$m_{D_1^+}$	$m_{D_{1s}}$
5.726 GeV	5.726 GeV	5.829 GeV	2.421 GeV	2.423 GeV	2.460 GeV
Quark masses [31]					
$m_{s\|2\text{GeV}}$	$m_b(m_b)$	$m_c(m_c)$	m_b^{pole}	m_c^{pole}	$m_b^{kin}(1\,\text{GeV})^\dagger$
92.9(7) MeV	4.18(4) GeV	1.27(2) GeV	4.78(6) GeV	1.67(7) GeV	4.53(6) GeV
Condensates					
$\langle\bar{q}q\rangle_{\|2\text{GeV}}$ [53]	$\langle\bar{s}s\rangle$ [54]	$\langle G^2\rangle$ [7, 8]	m_0^2 [55]		
$-(269(2)\,\text{MeV})^3$	$1.08(16)\langle\bar{q}q\rangle$	$0.012(4)\,\text{GeV}^4$	$0.8(2)\,\text{GeV}^2$		

Table 14. Summary of input parameters. † Value obtained by using the $\mathcal{O}(\alpha_s^2)$ conversion between the $\overline{\text{MS}}$ and the kinetic mass given in [38]. The uncertainty is obtained by adding in quadrature the uncertainty due to the $\overline{\text{MS}}$ mass and the conversion formula. For the meson masses we have not indicated an uncertainty as they are negligible. We refer to [3] for all the input concerning the photon DA that enters the light-cone sum rule computation.

$f_{B^*}^T, f_{B_1}^T$ results are new and comparison with the literature with regards to f_B, f_{B^*}, f_{B_1} is commented on at the beginning of section 4. We give the results in terms of the densities $\rho_{f_{B_{(i)}}}(s)$ and Wilson coefficients $c_j^{f_{B_{(i)}}}$ that enter (4.2). The densities are related to the correlation functions as follows

$$\rho_{f_B}(s) = \frac{1}{\pi}\frac{\text{Im}_s\Gamma_{f_B}(s)}{(m_b+m_q)^2}\,, \quad \rho_{f_{B^*}}(s) = \frac{1}{\pi}\text{Im}_s\Gamma_{f_{B^*}}(s)\,, \quad \rho_{f_{B^*}^T}(s) = \frac{1}{\pi}\text{Im}_s\Gamma_{f_{B^*}^T}(s)\,. \tag{B.1}$$

The Wilson coefficients are presented after integration and can therefore depend on the effective threshold. For comparison with the literature cf. footnote 13 in the main text.

The leading contribution to the local OPE is the perturbative one which we further decompose into LO and NLO parts

$$\rho(s) = \rho^{(0)}(s) + \frac{\alpha_s}{\pi}\rho^{(1)}(s) + \dots\,. \tag{B.2}$$

JHEP09(2021)023

At LO, including corrections due to the light quark mass to $\mathcal{O}(m_q^2)$, we find

$$\begin{aligned}
\rho_{f_B}^{(0)}(s) &= \frac{N_c}{8\pi^2}\, s\left(\bar{z}^2 + 2\,\frac{m_q}{m_b} z\bar{z} - 2\frac{m_q^2}{m_b^2} z\right), \\
\rho_{f_{B^*}}^{(0)}(s) &= \frac{N_c}{24\pi^2} s\left(\bar{z}^2(z+2) + 6\,\frac{m_q}{m_b} z\bar{z} - 3\frac{m_q^2}{m_b^2} z(z^2+1)\right), \\
\rho_{f_{B^*}^T}^{(0)}(s) &= \frac{N_c}{24\pi^2} s\left(\bar{z}^2(2z+1) + 6\frac{m_q}{m_b} z\bar{z} - 6\frac{m_q^2}{m_b^2} z^3\right),
\end{aligned} \tag{B.3}$$

whilst at NLO,

$$\rho_{f_B}^{(1)}(s) = \frac{N_c C_F}{16\pi^2} s\bar{z}\left[\frac{9}{2}\bar{z} + (z-3)(2z-1)\ln z + \bar{z}(2z-5+2\ln z)\ln\bar{z} + 4\bar{z}\mathrm{Li}_2(z) - (3z-1)r_S\right],$$

$$\begin{aligned}
\rho_{f_{B^*}}^{(1)}(s) = \frac{N_c C_F}{16\pi^2} s\Bigg[&1 - \frac{5}{2}z + \frac{2}{3}z^2 + \frac{5}{6}z^3 + \frac{1}{3}z(5z^2-4z-5)\ln z - \frac{1}{3}\bar{z}^2(5z+4-2(z+2)\ln z)\ln\bar{z} \\
&+ \frac{4}{3}\bar{z}^2(z+2)\mathrm{Li}_2(z) + z(z^2-1)r_S\Bigg],
\end{aligned}$$

$$\begin{aligned}
\rho_{f_{B^*}^T}^{(1)}(s) = \frac{N_c C_F}{96\pi^2} s\Bigg[&\frac{7}{3} + 2z - 15z^2 + \frac{32}{3}z^3 + 2(8z^3 - 11z^2 + 2z - 1)\ln z + 8\bar{z}^2(2z+1)\mathrm{Li}_2(z) \\
&- 2\bar{z}^2(8z+1-2(2z+1)\ln z)\ln\bar{z} - 2\bar{z}^2(2z+1)\ln\left(\frac{\mu_{\mathrm{UV}}^2}{m_b^2}\right) - 12z^2\bar{z}r_S\Bigg],
\end{aligned} \tag{B.4}$$

with the $\mathcal{O}(m_q)$ corrections given by,

$$\begin{aligned}
\delta_{m_q}\rho_{f_B}^{(1)}(s) = \frac{N_c C_F}{4\pi^2}\frac{m_q}{m_b} s\Bigg[&3z - 3z^2 + z(z^2 - 5z + 3)\ln z + z\bar{z}(z - 4 + \ln z)\ln\bar{z} \\
&+ 2z\bar{z}\mathrm{Li}_2(z) - \frac{1}{2}z(3z-2)r_S\Bigg],
\end{aligned}$$

$$\begin{aligned}
\delta_{m_q}\rho_{f_{B^*}}^{(1)}(s) = \frac{N_c C_F}{8\pi^2}\frac{m_q}{m_b} s\Bigg[&\frac{9}{2}z - 5z^2 + \frac{1}{2}z^3 - z(z^2 + 4z - 3)\ln z - z\bar{z}(z + 5 - 2\ln z)\ln\bar{z} \\
&+ 4z\bar{z}\mathrm{Li}_2(z) - z(2z-1)r_S\Bigg],
\end{aligned}$$

$$\begin{aligned}
\delta_{m_q}\rho_{f_{B^*}^T}^{(1)}(s) = \frac{N_c C_F}{4\pi^2}\frac{m_q}{m_b} s\Bigg[&3z - 3z^2 - z(z^2 + z - 1)\ln z - z\bar{z}(z + 2 - \ln z)\ln\bar{z} \\
&+ 2z\bar{z}\mathrm{Li}_2(z) + \frac{1}{4}\bar{z}z\ln\left(\frac{\mu_{\mathrm{UV}}^2}{m_b^2}\right) + \frac{1}{4}z(1-3z)r_S\Bigg],
\end{aligned} \tag{B.5}$$

JHEP09(2021)023

where $z \equiv m_b^2/s$. The $\mu_{\rm UV}$ dependence is consistent with the anomalous scaling (2.7).

The Borel subtracted non-perturbative contributions are given by,

$$
\begin{aligned}
c^{f_B}_{\langle\bar{q}q\rangle} &= -\Bigg[1-\frac{m_q}{2m_b}-\frac{m_b m_q}{2M^2} \\
&\quad +\frac{\alpha_s C_F}{2\pi}\left\{1+3\Gamma_0-\frac{3}{2}\ln\left(\frac{\mu^2_{\rm cond}}{m_b^2}\right)+\left(\frac{3}{2}-\frac{m_b^2}{M^2}\right) r_S\right\}\Bigg], \\
c^{f_{B^*}}_{\langle\bar{q}q\rangle} &= -\Bigg[1-\frac{m_b m_q}{2M^2} \\
&\quad +\frac{\alpha_s C_F}{2\pi}\left\{-1-\frac{m_b^2}{M^2}\Gamma_{-1}-\frac{3}{2}\ln\left(\frac{\mu^2_{\rm cond}}{m_b^2}\right)+\left(\frac{1}{2}-\frac{m_b^2}{M^2}\right) r_S\right\}\Bigg], \\
c^{f^T_{B^*}}_{\langle\bar{q}q\rangle} &= -\Bigg[1+\frac{m_q}{2m_b}-\frac{m_b m_q}{2M^2} \\
&\quad +\frac{\alpha_s C_F}{2\pi}\left\{-1-\Gamma_0-\ln\left(\frac{\mu^2_{\rm UV}}{m_b^2}\right)-\frac{3}{2}\ln\left(\frac{\mu^2_{\rm cond}}{m_b^2}\right)+\left(\frac{1}{2}-\frac{m_b^2}{M^2}\right) r_S\right\}\Bigg],
\end{aligned}
\tag{B.6}
$$

$$
\begin{aligned}
&c^{f_B}_{\langle G^2\rangle} = \frac{1}{12}\,, \qquad c^{f_{B^*}}_{\langle G^2\rangle} = -\frac{1}{12}\,, \qquad c^{f^T_{B^*}}_{\langle G^2\rangle} = -\frac{1}{12}\left(1+\frac{2m_b^2}{M^2}\Gamma_{-1}\right), \\
&c^{f_B}_{\langle\bar{q}Gq\rangle} = -\frac{1}{2}\left(1-\frac{m_b^2}{2M^2}\right), \quad c^{f_{B^*}}_{\langle\bar{q}Gq\rangle} = \frac{m_b^2}{4M^2}\,, \quad c^{f^T_{B^*}}_{\langle\bar{q}Gq\rangle} = \frac{1}{6}\left(1+\frac{3m_b^2}{2M^2}\right),
\end{aligned}
\tag{B.7}
$$

where the Borel parameter $M^2 \to M^2_{f_{B_{(i)}}}$ accordingly, and

$$
\Gamma_k = e^{\frac{m_b^2}{M^2}}\left(\Gamma\left(k,\frac{s_0}{M^2}\right)-\Gamma\left(k,\frac{m_b^2}{M^2}\right)\right), \tag{B.8}
$$

with $\Gamma(n,z)=\int_z^\infty dt\, t^{n-1}e^{-t}$ denoting the incomplete gamma function. The quantity

$$
r_S = \begin{cases} 3\ln\left(\frac{\mu_m^2}{m_b^2}\right)+4 & \overline{\rm MS} \\ 0 & \text{pole} \\ \frac{16}{3}\frac{\mu_{\rm kin}}{m_b}+2\frac{\mu^2_{\rm kin}}{m_b^2} & \text{kinetic} \end{cases}, \tag{B.9}
$$

is a factor that depends on the mass scheme. Above we have also included the leading light quark mass corrections to the LO quark condensate contribution. As mentioned in section 4.1, we have verified that the NLO scale dependence, in $\mu_{\rm UV}$ and $\mu_{\rm cond}$, is consistent with the LO expression.

JHEP09(2021)023

The SRs for the $J^P = 1^+$ decay constants can be obtained from the $J^P = 1^-$ ones by changing the sign of certain contributions according to their chirality,

$$\begin{aligned} \rho_{f_{B_1}^{(T)}} &= \rho_{f_{B^*}^{(T)}}\,, & c^{f_{B_1}^{(T)}}_{\langle\bar{q}q\rangle} &= -c^{f_{B^*}^{(T)}}_{\langle\bar{q}q\rangle}\,, \\ c^{f_{B_1}^{(T)}}_{\langle G^2\rangle} &= c^{f_{B^*}^{(T)}}_{\langle G^2\rangle}\,, & c^{f_{B_1}^{(T)}}_{\langle\bar{q}Gq\rangle} &= -c^{f_{B^*}^{(T)}}_{\langle\bar{q}Gq\rangle}\,, \end{aligned} \tag{B.10}$$

in spirit with the parity doubling proposal in [34].

C Double dispersion relation

In computing the densities we are faced with the following problem. We have an analytic function $F(p_B^2, q^2)$ for which it is straightforward to derive a single dispersion relation

$$F(p_B^2, q^2) = \int_{m_b^2}^{\infty} ds \frac{\rho(s, q^2)}{s - p_B^2 - i0}\,, \tag{C.1}$$

where the density is formally given by $\pi\rho(s, q^2) = \mathrm{Im}_s F(s, q^2)$. The density can be decomposed into poles in $s = q^2$ such that

$$F(p_B^2, q^2) = \sum_{n\geq 0} F_n(p_B^2, q^2)\,, \qquad F_n(p_B^2, q^2) = \int_{m_b^2}^{\infty} ds \frac{\rho_n(s, q^2)}{(s - p_B^2 - i0)(s - q^2)^n}\,. \tag{C.2}$$

The singularities in $s = q^2$ are of so-called second type, which are special solutions of the Landau equations [20, 22]. It is our task to write the q^2-dependence of (C.2) dispersively, say in an integral over dt, and impose a continuum subtraction. The duality interval is discussed in (3.17) in the main text.

C.1 Leading order

At LO in PT the ρ_i themselves contain no non-trivial cuts. Consequently, the poles provide the only contribution to the discontinuity in q^2, allowing us to write

$$F_n(p_B^2, q^2) = \frac{1}{\Gamma(n)} \int_{m_b^2}^{\bar{\delta}_s^{(a)}(m_b^2)} ds \int_{m_b^2}^{\bar{\delta}_t^{(a)}(s)} dt\, \frac{\rho_n(s,t)\delta^{(n-1)}(t-s)}{(s - p_B^2)(t - q^2)}\,, \tag{C.3}$$

where the continuum subtraction has been implemented as in (3.17). Partially integrating and performing the integrals over the δ-functions we obtain,

$$\begin{aligned} F_n(p_B^2, q^2) = {} & \frac{(-1)^{n-1}}{\Gamma(n)} \int_{m_b^2}^{\sigma_0^{(a)}} ds\, \partial_t^{(n-1)} \left(\rho_n(s,t) g(s,t)\right)\big|_{t\to s} \\ & + \frac{1}{\Gamma(n)} \sum_{\ell=1}^{n-1} (-1)^{\ell-1} \left(\frac{\tilde{s}_0^a}{\tilde{s}_0^a + \tilde{t}_0^a}\right)^{n-\ell} \partial_s^{(n-\ell-1)} \left(\partial_t^{(\ell-1)} [\rho_n(s,t) g(s,t)]\big|_{t\to\bar{\delta}_t^{(a)}(s)}\right)\Big|_{s\to\sigma_0^{(a)}}\,, \end{aligned} \tag{C.4}$$

with $g(s,t) = 1/(s - p_B^2 - i0)(t - q^2 - i0)$. The double Borel transform can then be trivially computed by taking $g(s,t) \to \hat{g}(s,t) = e^{-s/M_1^2 - t/M_2^2}$.

JHEP09(2021)023

C.2 Next-to-leading order

At NLO the situation is complicated by $\rho_n(s,q^2)$ containing polylogarithmic terms that contribute to the discontinuity in q^2 in addition to the poles. To lessen this complication only provide a derivation of the double dispersion relation for $n \leq 3$, which is sufficient for the case at hand where the density can be decomposed as

$$\rho(s,q^2) = \rho_0(s,q^2) + \frac{\rho_1(s,q^2)}{(s-q^2)} + \frac{\rho_2(s,q^2)}{(s-q^2)^2} + \frac{\rho_3(s,q^2)}{(s-q^2)^3}\,. \tag{C.5}$$

Without committing to a specific value for the parameter a, we obtain formally a double dispersion relation, with continuum subtraction as in (3.17),

$$\begin{aligned} F^{\tilde{t}_0}_{\tilde{s}_0}(p_B^2,q^2) = &\int_{m_b^2}^{\bar{\delta}_t^{(a)}(m_b^2)} \frac{dt}{t-q^2} P_s \int_{m_b^2}^{\bar{\delta}_s^{(a)}(t)} \frac{ds}{s-p_B^2}\hat{\rho}(s,t) + P_{\sigma_0^{(a)}} \int_{m_b^2}^{\bar{\delta}_t^{(a)}(m_b^2)} \frac{dt}{t-q^2}\,\bar{\rho}(t,p_B^2,q^2,\tilde{s}_0,\tilde{t}_0) \\ &+ \int_{m_b^2}^{\sigma_0^{(a)}} \frac{ds}{s-p_B^2}\tilde{\rho}(s,q^2) + C(p_B^2,q^2,\tilde{s}_0,\tilde{t}_0)\,, \end{aligned} \tag{C.6}$$

where $F^{\tilde{t}_0}_{\tilde{s}_0} \to F$ as $\tilde{s}_0, \tilde{t}_0 \to \infty$. The function $\bar{\rho}(t,p_B^2,q^2,\tilde{s}_0,\tilde{t}_0)$ arises from partial integration in s in order to reduce the integrands to simple $1/(s-t)$-poles. The natural order of integration has been reversed in an attempt to remove complications at the lower integration boundary when integrating-by-parts. The order-1 poles, hidden in $\hat{\rho}(s,t)$ and $\bar{\rho}(t,p_B^2,q^2,\tilde{s}_0,\tilde{t}_0)$, are handled with the principle part prescription, with P_x denoting the principal value w.r.t. to $1/(x-t)$. In terms of ρ_i, the above functions read

$$\hat{\rho}(s,t) = \frac{1}{\pi}\left(\mathrm{Im}_t\rho_0 + \frac{1}{s-t}\left[\mathrm{Im}_t\rho_1 - (s-p_B^2)\left(\left(\frac{\mathrm{Im}_t\rho_2}{s-p_B^2}\right)' + \frac{1}{2}\left(\frac{\mathrm{Im}_t\rho_3}{s-p_B^2}\right)''\right)\right]\right),$$

$$\begin{aligned} \bar{\rho}(t,p_B^2,q^2,\tilde{s}_0,\tilde{t}_0) = &-\frac{1}{\pi}\left[\frac{\mathrm{Im}_t\rho_2}{(s-p_B^2)(s-t)} + \frac{1}{2}\frac{1}{s-t}\left(\frac{\mathrm{Im}_t\rho_3}{s-p_B^2}\right)'\right]\Bigg|_{s=\bar{\delta}_s^{(a)}(t)} \\ &-\frac{1}{\pi}\left[\frac{1}{2}\frac{t-q^2}{\bar{\delta}_s^{(a)}(t)-t}\partial_t\left(\frac{\mathrm{Im}_t\rho_3}{(t-q^2)(\bar{\delta}_s^{(a)}(t)-p_B^2)(1-\partial_t\bar{\delta}_s^{(a)}(t))}\right)\right], \end{aligned}$$

$$\tilde{\rho}(s,q^2) = \left[\frac{\mathrm{Re}\rho_1}{s-q^2} - \left(\frac{\mathrm{Re}\rho_2}{t-q^2}\right)' + \frac{1}{2}\left(\frac{\mathrm{Re}\rho_3}{t-q^2}\right)''\right]_{t\to s},$$

$$\begin{aligned} C(p_B^2,q^2,\tilde{s}_0,\tilde{t}_0) = &-\frac{1}{\pi}\left[\frac{1}{2}\frac{\mathrm{Im}_t\rho_3\big|_{s=\bar{\delta}_s^{(a)}(t)}}{(t-q^2)(\bar{\delta}_s^{(a)}(t)-p_B^2)(\bar{\delta}_s^{(a)}(t)-t)(1-\partial_t\bar{\delta}_s^{(a)}(t))}\right]\Bigg|_{t=m_b^2}^{t=\bar{\delta}_t^{(a)}(m_b^2)} \\ &+\frac{\tilde{s}_0^a}{\tilde{s}_0^a+\tilde{t}_0^a}\left\{\frac{\mathrm{Re}\rho_2\big|_{s,t\to\sigma_0^{(a)}}}{(\sigma_0^{(a)}-p_B^2)(\sigma_0^{(a)}-q^2)} + \frac{1}{2}\partial_t\left(\frac{\mathrm{Re}\rho_3}{(\sigma_0^{(a)}-p_B^2)(t-q^2)}\right)\Bigg|_{s,t\to\sigma_0^{(a)}}\right. \\ &\left.-\frac{1}{2}\frac{\tilde{s}_0^a}{\tilde{s}_0^a+\tilde{t}_0^a}\left(\frac{\mathrm{Re}\rho_3\big|_{t\to\bar{\delta}_t^{(a)}(s)}}{(s-p_B^2)(\bar{\delta}_t^{(a)}(s)-q^2)}\right)'\Bigg|_{s\to\sigma_0^{(a)}}\right\}, \end{aligned} \tag{C.7}$$

JHEP09(2021)023

where the prime denotes a derivative w.r.t. the variable s and $\rho_i \equiv \rho_i(s,t)$. Above we have utilised the fact that $\mathrm{Im}_t\rho_i(m_b^2,t) = (\mathrm{Im}_t\rho_i(s,t))'\,|_{s\to m_b^2} = 0$. Application of the principal part to the double integral of (C.6) leads to a technical splitting of the integration region, which can be most clearly seen in figure 1. Schematically, one has

$$\int_{m_b^2}^{\bar{\delta}_t^{(a)}(m_b^2)} dt\; P_s \int_{m_b^2}^{\bar{\delta}_s^{(a)}(t)} ds \equiv \int_{m_b^2}^{\sigma_0^{(a)}} dt \left(\int_{m_b^2}^{t-\epsilon} ds + \int_{t+\epsilon}^{\bar{\delta}_s^{(a)}(t)} ds \right) + \int_{\sigma_0^{(a)}}^{\bar{\delta}_t^{(a)}(m_b^2)} dt \int_{m_b^2}^{\bar{\delta}_s^{(a)}(t)} ds\,, \tag{C.8}$$

which corresponds to triangles B, A, and C of figure 1 respectively.

D Subtracted Borel transformation of tree level DA terms

We're faced with the problem of finding the double Borel transformation of the following generic function ($\ell = 0, 1$)

$$F_{n,\ell}(p_B^2, q^2) \equiv \int_0^1 du \frac{(q^2)^\ell f_n(u)}{S^n}\,, \tag{D.1}$$

with $S \equiv m_b^2 - up_B^2 - \bar{u}q^2$ and $f_n(u)$ some DA multiplying u-dependent prefactors. We explain the meaning of the silent label n further below. The formal solution is straightforward

$$\begin{aligned}\hat{F}_{n,\ell}(M_1^2, M_2^2) &\equiv \mathcal{B}^{q^2}_{sub.M_2^2}\mathcal{B}^{p_B^2}_{sub.M_1^2} F_{n,\ell}(p_B^2, q^2) \\ &= \int_{m_b^2}^{\bar{\delta}_s^{(a)}(m_b^2)} ds \int_{m_b^2}^{\bar{\delta}_t^{(a)}(s)} dt e^{-\left(\frac{s}{M_1^2}+\frac{t}{M_2^2}\right)} \rho_{F_{n,\ell}}(s,t)\,,\end{aligned} \tag{D.2}$$

where $\bar{\delta}_s^{(a)}(t)$ and $\bar{\delta}_t^{(a)}(s)$ are defined in section 3.4.1 and $(2\pi i)^2\rho_{F_{n,\ell}}((s,t) = \mathrm{disc}_s\mathrm{disc}_t$ $F_{n,\ell}(s,t)$ is the density of the double dispersion representation of

$$F_{n,\ell}(p_B^2, q^2) = \int_{m_b^2}^\infty ds \int_{m_b^2}^\infty dt \frac{\rho_{F_{n,\ell}}(s,t)}{(s-p_B^2)(t-q^2)}\,. \tag{D.3}$$

If one commits to a specific function $f(u)$ the du-integral can be done and its double dispersion integral can be worked out in a relatively straightforward manner. In the literature the case $F_1^{(0)}$ has been worked out more generically [56] which we generalise to $F_n^{(0,1)}$. The function f_n is expanded, anticipating a change of variable, as

$$f_n(u) = \sum_{k\geq 0} c_{\tilde{k}}\bar{u}^{\tilde{k}}\,, \quad \tilde{k} \equiv k + (n-1)\,, \tag{D.4}$$

and

$$f_n^{(n-1)}(u) = \left(\frac{d}{du}\right)^{n-1} f_n(u) = (-1)^{(n-1)} \sum_{k\geq 0} \bar{c}_k \bar{u}^k\,, \tag{D.5}$$

where $\bar{c}_k \equiv \frac{\tilde{k}!}{k!}c_{\tilde{k}}$. Above we have assumed that $f_n(u) \propto (u\bar{u})^{n-1}(1 + \mathcal{O}(u,\bar{u}))$ which is a sufficient condition for the function $F_{n,\ell}(p_B^2, q^2)$ (D.1) to be free from $1/(p_B^2 - q^2)$

JHEP09(2021)023

singularities.[16] The first dispersion representation can be obtained by a change of variable

$$u = \frac{m_b^2 - q^2}{s - q^2}\,, \quad \bar{u} = \frac{s - m_b^2}{s - q^2}\,, \tag{D.6}$$

for which

$$F_{n,0}(p_B^2, q^2) = \frac{1}{\Gamma[n]} \sum_{k\geq 0} \bar{c}_k \int_{m_b^2}^{\infty} ds \frac{(s - m_b^2)^k}{(s - p_B^2)(s - q^2)^{1+\tilde{k}}}\,. \tag{D.7}$$

At this level any further singularities are induced by $1/(s-q^2)^{1+\tilde{k}}$ and, as discussed in the previous section, correspond to so-called second type singularities. These singularities cannot appear for $F_{n,0}(p_B^2, q^2)$ itself which is a fact that we have used in making the specific ansatz (D.4). The double dispersion relation then reads

$$F_{n,0}(p_B^2, q^2) = \frac{1}{\Gamma[n]} \sum_{k\geq 0} \frac{\bar{c}_k (-1)^{\tilde{k}}}{\tilde{k}!} \int_{m_b^2}^{\infty} ds \int_{m_b^2}^{\infty} dt \frac{(s - m_b^2)^k \delta^{(\tilde{k})}(s - t)}{(s - p_B^2)(t - q^2)}\,, \tag{D.8}$$

and its Borel subtracted form assumes the form

$$\hat{F}_{n,0}(M_1^2, M_2^2) = \frac{1}{\Gamma[n]} \sum_{k\geq 0} \frac{\bar{c}_k (-1)^{\tilde{k}}}{\tilde{k}!} \int_{m_b^2}^{\bar{\delta}_s^{(a)}(m_b^2)} ds \int_{m_b^2}^{\bar{\delta}_t^{(a)}(s)} dt\, e^{-\left(\frac{s}{M_1^2} + \frac{t}{M_2^2}\right)} (s - m_b^2)^k \delta^{(\tilde{k})}(s - t)\,. \tag{D.9}$$

We further decompose

$$\hat{F}_{n,0} = I[\hat{F}]_{n,0} + \delta[\hat{F}]_{n,0}\,, \tag{D.10}$$

where $I[\dots]$ and $\delta[\dots]$ correspond to the integral and boundary terms that arise from integration by parts. The former are easily evaluated to

$$I[\hat{F}]_{n,0} = \frac{(\hat{M}^2)^{2-n} e^{-\hat{m}_b^2}}{\Gamma[n]} \sum_{k\geq 0} c_{\tilde{k}}\, \bar{u}_0^{\tilde{k}} \left(1 - \Omega_{k+1,\sigma_0^{(a)}}\right)\,, \tag{D.11}$$

$$I[\hat{F}]_{n,1} = \frac{(\hat{M}^2)^{3-n} e^{-\hat{m}_b^2}}{\Gamma[n]} \sum_{k\geq 0} c_{\tilde{k}}\, \bar{u}_0^{\tilde{k}} \left[\left(\hat{m}_b^2 - \tilde{k}\bar{u}_0^{-1}\right)\left(1 - \Omega_{k+1,\sigma_0^{(a)}}\right) + (k+1)\left(1 - \Omega_{k+2,\hat{\sigma}_0^{(a)}}\right)\right]\,,$$

where

$$u_0 = \frac{M_2^2}{M_1^2 + M_2^2}\,, \qquad \hat{M}^2 = \frac{M_2^2 M_1^2}{M_1^2 + M_2^2}\,, \tag{D.12}$$

and

$$\Omega_{k,\hat{\sigma}_0^{(a)}} = \frac{\Gamma[k, \hat{\sigma}_0^{(a)} - \hat{m}_b^2]}{\Gamma[k]}\,, \tag{D.13}$$

with $\sigma_0^{(a)}$ defined in (3.17) and $\hat{m}_b^2 \equiv m_b^2/\hat{M}^2$. Above we have given the result for $\hat{F}_{n,1}$ in addition which does not pose any new technical challenges as one can simply replace $q^2 = s - (s - q^2)$ and treat the two terms separately.

[16] There are some cases where this condition is not met do to the presence of $\ln u$ and $\ln \bar{u}$ terms, namely $\{\mathbb{A}, \mathcal{T}_{1,3}^{(1)}\}$ and the mass corrections to $\{\tilde{\Psi}_{(a)}, \Psi_{(v)}^{(1)}\}$, for which an accurate polynomial fit can be made.

JHEP09(2021)023

The boundary terms evaluate to

$$\delta[\hat{F}]_{n,0} = \frac{1}{\Gamma(n)} \sum_{k\geq 0} \bar{c}_k X_{\tilde{k}k}[1]\,,$$
$$\delta[\hat{F}]_{n,1} = \frac{1}{\Gamma(n)} \sum_{k\geq 0} \bar{c}_k \left(X_{\tilde{k}k}[s] - X_{(\tilde{k}-1)k}[1] \right)\,, \tag{D.14}$$

$X_{\tilde{k}k}[g(s)]$ is the functional

$$X_{\tilde{k}k}[g(s)] = \sum_{l=1}^{\tilde{k}} \frac{(M_2^2)^{1-l}}{\tilde{k}!} \left(\frac{\tilde{s}_0^a}{\tilde{s}_0^a + \tilde{t}_0^a} \right)^{\tilde{k}-l+1} \partial_s^{\tilde{k}-l} \left[e^{-\left(\frac{s}{M_1^2} + \frac{\bar{\delta}_t^{(a)}(s)}{M_2^2} \right)} (s-m_b^2)^k g(s) \right]_{s=\sigma_0^{(a)}}\,. \tag{D.15}$$

For further comparison with the literature we adopt the $\tilde{s}_0, \tilde{t}_0 \to \infty$ limit, for which $\Omega_{k,\hat{\sigma}_0^{(a)}} \to 0$, to find

$$\hat{F}_{n,0} \xrightarrow{\tilde{s}_0,\tilde{t}_0\to\infty} \frac{(\hat{M}^2)^{2-n} e^{-\hat{m}_b^2}}{\Gamma[n]} f(u_0)\,,$$
$$\hat{F}_{n,1} \xrightarrow{\tilde{s}_0,\tilde{t}_0\to\infty} \frac{(\hat{M}^2)^{3-n} e^{-\hat{m}_b^2}}{\Gamma[n]} \Big(f(u_0)(\hat{m}_b^2 + 2 - n) + (1-\bar{u}_0) f'(u_0) \Big)\,, \tag{D.16}$$

where we used $f(u_0) = \sum_{k\geq 0} c_{\tilde{k}} \bar{u}_0^{\tilde{k}}$ and $f'(u_0) = -\sum_{k\geq 0} c_{\tilde{k}} \tilde{k} \bar{u}_0^{\tilde{k}-1}$.

D.1 The special case $a = 1$ and $\tilde{s}_0 = \tilde{t}_0$, $M_1^2 = M_2^2$

For the case $a = 1$ and $\tilde{s}_0 = \tilde{t}_0$, $M_1^2 = M_2^2 \equiv 2\bar{M}^2$ with $\hat{M}^2 \to \bar{M}^2$ and $u_0 \to 1/2$, which is the one considered in the literature [56], there are miraculous simplifications. First the exponential factor in (D.15) becomes s-independent and (D.14) assumes a more manageable form,

$$\delta[\hat{F}]_{n,0} \xrightarrow{a=1,M_1^2=M_2^2} \frac{(\hat{M}^2)^{2-n} e^{-\hat{m}_b^2}}{\Gamma[n]} \sum_{k\geq 0} \frac{c_{\tilde{k}}}{2^{\tilde{k}}} \left(\Omega_{k+1,\hat{s}_0} - \delta_{n1}\, \Omega_{1,\hat{s}_0} \right)\,,$$
$$\delta[\hat{F}]_{n,1} \xrightarrow{a=1,M_1^2=M_2^2} \frac{(\hat{M}^2)^{3-n} e^{-\hat{m}_b^2}}{\Gamma[n]} \sum_{k\geq 0} \frac{c_{\tilde{k}}}{2^{\tilde{k}}} \Big((k+1)(\Omega_{k+2,\hat{s}_0} - \delta_{n2}\Omega_{1,\hat{s}_0} - \delta_{n1}\Omega_{2,\hat{s}_0}) +$$
$$\hat{m}^2(\Omega_{k+1,\hat{s}_0} - \delta_{n1}\Omega_{1,\hat{s}_0}) - 2\tilde{k}(\Omega_{k+1,\hat{s}_0} - \delta_{n2}\Omega_{1,\hat{s}_0} - \delta_{n1}\Omega_{2,\hat{s}_0}) \Big)\,, \tag{D.17}$$

where $\hat{s}_0 = \tilde{s}_0/2\hat{M}^2$. Secondly, by adding (D.11) and (D.17) we arrive at a form where

$$\hat{F}_{n,0} = \frac{(\hat{M}^2)^{2-n} e^{-\hat{m}_b^2}}{\Gamma[n]} \sum_{k\geq 0} \frac{c_{\tilde{k}}}{2^{\tilde{k}}} \left(1 - \delta_{n1}\, \Omega_{1,\hat{s}_0} \right) = \frac{(\hat{M}^2)^{2-n}}{(n-1)!} f_n\left(\frac{1}{2}\right) \left(e^{-\hat{m}_b^2} - \delta_{n1} e^{-\hat{s}_0} \right)\,,$$
$$\hat{F}_{n,1} = \frac{(\hat{M}^2)^{3-n} e^{-\hat{m}_b^2}}{\Gamma[n]} \sum_{k\geq 0} \frac{c_{\tilde{k}}}{2^{\tilde{k}}} \Big(\hat{m}_b^2 (1 - \delta_{n1}\Omega_{1,\hat{s}_0}) + (2 - n - \tilde{k})(1 - \delta_{n2}\Omega_{1,\hat{s}_0} - \delta_{n1}\Omega_{2,\hat{s}_0}) \Big)$$
$$= \frac{(\hat{M}^2)^{3-n}}{(n-1)!} \Bigg[\hat{m}_b^2 f_n\left(\frac{1}{2}\right) \left(e^{-\hat{m}_b^2} - \delta_{n1} e^{-\hat{s}_0} \right)$$
$$+ \left((2-n) f_n\left(\frac{1}{2}\right) + \frac{f_n'(\frac{1}{2})}{2} \right) \left(e^{-\hat{m}_b^2} - e^{-\hat{s}_0} (\delta_{n2} + \delta_{n1}(1 + \hat{s}_0 - \hat{m}_b^2)) \right) \Bigg]\,, \tag{D.18}$$

JHEP09(2021)023

for which the k-dependence in the Ω-terms cancels! It is remarkable that for this special case the continuum subtraction vanishes for $n > 1$ ($n > 2$) in $\hat{F}_{n,0}$ ($\hat{F}_{n,1}$) and accidentally renders some results in the literature, where continuum subtractions have been neglected, more accurate. Note that $\hat{F}_{1,0}$ has previously been computed in appendix B of [56] and we agree with their result.

Open Access. This article is distributed under the terms of the Creative Commons Attribution License (CC-BY 4.0), which permits any use, distribution and reproduction in any medium, provided the original author(s) and source are credited.

References

[1] Y.Y. Balitsky, V.M. Braun and A.V. Kolesnichenko, *The decay $\Sigma^+ \to p\gamma$ in QCD: Bilocal corrections in a variable magnetic field and the photon wave functions*, *Sov. J. Nucl. Phys.* **48** (1988) 348 [INSPIRE].

[2] P. Colangelo and A. Khodjamirian, *QCD sum rules, a modern perspective*, hep-ph/0010175 [INSPIRE].

[3] T. Janowski, B. Pullin and R. Zwicky, *Charged and Neutral $\bar{B}_{u,d,s} \to \gamma$ Form Factors from Light Cone Sum Rules at NLO*, arXiv:2106.13616 [INSPIRE].

[4] J. Albrecht, E. Stamou, R. Ziegler and R. Zwicky, *Probing flavoured Axions in the Tail of $B_q \to \mu^+\mu^-$*, arXiv:1911.05018 [INSPIRE].

[5] S. Di Vita, P. Mastrolia, A. Primo and U. Schubert, *Two-loop master integrals for the leading QCD corrections to the Higgs coupling to a W pair and to the triple gauge couplings ZWW and γ^*WW*, *JHEP* **04** (2017) 008 [arXiv:1702.07331] [INSPIRE].

[6] I.I.Y. Bigi, M.A. Shifman, N.G. Uraltsev and A.I. Vainshtein, *The Pole mass of the heavy quark. Perturbation theory and beyond*, *Phys. Rev. D* **50** (1994) 2234 [hep-ph/9402360] [INSPIRE].

[7] M.A. Shifman, A.I. Vainshtein and V.I. Zakharov, *QCD and Resonance Physics. Theoretical Foundations*, *Nucl. Phys. B* **147** (1979) 385 [INSPIRE].

[8] M.A. Shifman, A.I. Vainshtein and V.I. Zakharov, *QCD and Resonance Physics: Applications*, *Nucl. Phys. B* **147** (1979) 448 [INSPIRE].

[9] T.M. Aliev, D.A. Demir, E. Iltan and N.K. Pak, *Radiative $B^* \to B\gamma$ and $D^* \to D\gamma$ decays in light cone QCD sum rules*, *Phys. Rev. D* **54** (1996) 857 [hep-ph/9511362] [INSPIRE].

[10] H.-D. Li, C.-D. Lü, C. Wang, Y.-M. Wang and Y.-B. Wei, *QCD calculations of radiative heavy meson decays with subleading power corrections*, *JHEP* **04** (2020) 023 [arXiv:2002.03825] [INSPIRE].

[11] D. Becirevic and B. Haas, *$D^* \to D\pi$ and $D^* \to D\gamma$ decays: Axial coupling and Magnetic moment of D^* meson*, *Eur. Phys. J. C* **71** (2011) 1734 [arXiv:0903.2407] [INSPIRE].

[12] G.C. Donald, C.T.H. Davies, J. Koponen and G.P. Lepage, *Prediction of the D_s^* width from a calculation of its radiative decay in full lattice QCD*, *Phys. Rev. Lett.* **112** (2014) 212002 [arXiv:1312.5264] [INSPIRE].

[13] M. Jamin and B.O. Lange, *f_B and f_{B_s} from QCD sum rules*, *Phys. Rev. D* **65** (2002) 056005 [hep-ph/0108135] [INSPIRE].

JHEP09(2021)023

[14] P. Gelhausen, A. Khodjamirian, A.A. Pivovarov and D. Rosenthal, *Decay constants of heavy-light vector mesons from QCD sum rules*, *Phys. Rev. D* **88** (2013) 014015 [*Erratum ibid.* **89** (2014) 099901] [*Erratum ibid.* **91** (2015) 099901] [arXiv:1305.5432] [INSPIRE].

[15] Z.-G. Wang, *Analysis of the masses and decay constants of the heavy-light mesons with QCD sum rules*, *Eur. Phys. J. C* **75** (2015) 427 [arXiv:1506.01993] [INSPIRE].

[16] D. Becirevic, V. Lubicz, F. Sanfilippo, S. Simula and C. Tarantino, *D-meson decay constants and a check of factorization in non-leptonic B-decays*, *JHEP* **02** (2012) 042 [arXiv:1201.4039] [INSPIRE].

[17] ETM collaboration, *Masses and decay constants of $D^*_{(s)}$ and $B^*_{(s)}$ mesons with $N_f = 2+1+1$ twisted mass fermions*, *Phys. Rev. D* **96** (2017) 034524 [arXiv:1707.04529] [INSPIRE].

[18] J.F. Amundson et al., *Radiative D* decay using heavy quark and chiral symmetry*, *Phys. Lett. B* **296** (1992) 415 [hep-ph/9209241] [INSPIRE].

[19] G. Isidori, S. Nabeebaccus and R. Zwicky, *QED corrections in $\overline{B} \to \overline{K}\ell^+\ell^-$ at the double-differential level*, *JHEP* **12** (2020) 104 [arXiv:2009.00929] [INSPIRE].

[20] R. Zwicky, *A brief Introduction to Dispersion Relations and Analyticity*, in *Quantum Field Theory at the Limits: from Strong Fields to Heavy Quarks*, pp. 93–120 (2017) [DOI] [arXiv:1610.06090] [INSPIRE].

[21] V.M. Braun, G.P. Korchemsky and D. Müller, *The Uses of conformal symmetry in QCD*, *Prog. Part. Nucl. Phys.* **51** (2003) 311 [hep-ph/0306057] [INSPIRE].

[22] C. Itzykson and J. Zuber, *Quantum Field Theory*, International Series In Pure and Applied Physics, McGraw-Hill, New York (1980) [INSPIRE].

[23] A. Khodjamirian, B. Melić, Y.-M. Wang and Y.-B. Wei, *The $D^*D\pi$ and $B^*B\pi$ couplings from light-cone sum rules*, *JHEP* **03** (2021) 016 [arXiv:2011.11275] [INSPIRE].

[24] M. Neubert, *Heavy meson form-factors from QCD sum rules*, *Phys. Rev. D* **45** (1992) 2451 [INSPIRE].

[25] B. Blok and M.A. Shifman, *The Isgur-Wise function in the small velocity limit*, *Phys. Rev. D* **47** (1993) 2949 [hep-ph/9207217] [INSPIRE].

[26] C. Hambrock, G. Hiller, S. Schacht and R. Zwicky, *$B \to K^\star$ form factors from flavor data to QCD and back*, *Phys. Rev. D* **89** (2014) 074014 [arXiv:1308.4379] [INSPIRE].

[27] A. Bharucha, D.M. Straub and R. Zwicky, *$B \to V\ell^+\ell^-$ in the Standard Model from light-cone sum rules*, *JHEP* **08** (2016) 098 [arXiv:1503.05534] [INSPIRE].

[28] P. Colangelo, F. De Fazio and G. Nardulli, *Radiative heavy meson transitions*, *Phys. Lett. B* **316** (1993) 555 [hep-ph/9307330] [INSPIRE].

[29] C.-Y. Cheung and C.-W. Hwang, *Strong and radiative decays of heavy mesons in a covariant model*, *JHEP* **04** (2014) 177 [arXiv:1401.3917] [INSPIRE].

[30] J.L. Goity and W. Roberts, *Radiative transitions in heavy mesons in a relativistic quark model*, *Phys. Rev. D* **64** (2001) 094007 [hep-ph/0012314] [INSPIRE].

[31] Particle Data Group collaboration, *Review of Particle Physics*, *PTEP* **2020** (2020) 083C01 [INSPIRE].

[32] Y.G. Aditya, K.J. Healey and A.A. Petrov, *Faking $B_s \to \mu^+\mu^-$*, *Phys. Rev. D* **87** (2013) 074028 [arXiv:1212.4166] [INSPIRE].

JHEP09(2021)023

[33] A. Desiderio et al., *First lattice calculation of radiative leptonic decay rates of pseudoscalar mesons*, *Phys. Rev. D* **103** (2021) 014502 [arXiv:2006.05358] [INSPIRE].

[34] J. Gratrex and R. Zwicky, *Parity Doubling as a Tool for Right-handed Current Searches*, *JHEP* **08** (2018) 178 [arXiv:1804.09006] [INSPIRE].

[35] FLAVOUR LATTICE AVERAGING GROUP collaboration, *FLAG Review 2019: Flavour Lattice Averaging Group (FLAG)*, *Eur. Phys. J. C* **80** (2020) 113 [arXiv:1902.08191] [INSPIRE].

[36] W. Lucha, D. Melikhov and S. Simula, *Decay constants of heavy pseudoscalar mesons from QCD sum rules*, *J. Phys. G* **38** (2011) 105002 [arXiv:1008.2698] [INSPIRE].

[37] A. Bazavov et al., *B- and D-meson leptonic decay constants from four-flavor lattice QCD*, *Phys. Rev. D* **98** (2018) 074512 [arXiv:1712.09262] [INSPIRE].

[38] P. Gambino, A. Melis and S. Simula, *Extraction of heavy-quark-expansion parameters from unquenched lattice data on pseudoscalar and vector heavy-light meson masses*, *Phys. Rev. D* **96** (2017) 014511 [arXiv:1704.06105] [INSPIRE].

[39] C. Hughes, C.T.H. Davies and C.J. Monahan, *New methods for B meson decay constants and form factors from lattice NRQCD*, *Phys. Rev. D* **97** (2018) 054509 [arXiv:1711.09981] [INSPIRE].

[40] C. McNeile, C.T.H. Davies, E. Follana, K. Hornbostel and G.P. Lepage, *High-Precision f_{B_s} and HQET from Relativistic Lattice QCD*, *Phys. Rev. D* **85** (2012) 031503 [arXiv:1110.4510] [INSPIRE].

[41] Y.-B. Yang et al., *Charm and strange quark masses and f_{D_s} from overlap fermions*, *Phys. Rev. D* **92** (2015) 034517 [arXiv:1410.3343] [INSPIRE].

[42] FERMILAB LATTICE and MILC collaborations, *B- and D-meson decay constants from three-flavor lattice QCD*, *Phys. Rev. D* **85** (2012) 114506 [arXiv:1112.3051] [INSPIRE].

[43] P.A. Boyle, L. Del Debbio, A. Jüttner, A. Khamseh, F. Sanfilippo and J.T. Tsang, *The decay constants f_D and f_{D_s} in the continuum limit of $N_f = 2+1$ domain wall lattice QCD*, *JHEP* **12** (2017) 008 [arXiv:1701.02644] [INSPIRE].

[44] C.T.H. Davies, C. McNeile, E. Follana, G.P. Lepage, H. Na and J. Shigemitsu, *Update: Precision D_s decay constant from full lattice QCD using very fine lattices*, *Phys. Rev. D* **82** (2010) 114504 [arXiv:1008.4018] [INSPIRE].

[45] H. Na, C.T.H. Davies, E. Follana, G.P. Lepage and J. Shigemitsu, *$|V_{cd}|$ from D Meson Leptonic Decays*, *Phys. Rev. D* **86** (2012) 054510 [arXiv:1206.4936] [INSPIRE].

[46] W. Lucha, D. Melikhov and S. Simula, *Isospin breaking in the decay constants of heavy mesons from QCD sum rules*, *Phys. Lett. B* **765** (2017) 365 [arXiv:1609.05050] [INSPIRE].

[47] ETM collaboration, *Mass of the b quark and B -meson decay constants from $N_f = 2+1+1$ twisted-mass lattice QCD*, *Phys. Rev. D* **93** (2016) 114505 [arXiv:1603.04306] [INSPIRE].

[48] HPQCD collaboration, *B-Meson Decay Constants from Improved Lattice Nonrelativistic QCD with Physical u, d, s, and c Quarks*, *Phys. Rev. Lett.* **110** (2013) 222003 [arXiv:1302.2644] [INSPIRE].

[49] W. Lucha, D. Melikhov and S. Simula, *Accurate decay-constant ratios f_{B^*}/f_B and $f_{B_s^*}/f_{B_s}$ from Borel QCD sum rules*, *Phys. Rev. D* **91** (2015) 116009 [arXiv:1504.03017] [INSPIRE].

[50] D. Becirevic, A. Le Yaouanc, A. Oyanguren, P. Roudeau and F. Sanfilippo, *Insight into $D/B \to \pi\ell\nu_\ell$ decay using the pole models*, arXiv:1407.1019 [INSPIRE].

JHEP09(2021)023

[51] HPQCD collaboration, *B-meson decay constants: a more complete picture from full lattice QCD*, *Phys. Rev. D* **91** (2015) 114509 [arXiv:1503.05762] [INSPIRE].

[52] D. Becirevic, B. Haas and E. Kou, *Soft Photon Problem in Leptonic B-decays*, *Phys. Lett. B* **681** (2009) 257 [arXiv:0907.1845] [INSPIRE].

[53] G.S. Bali et al., *Magnetic susceptibility of QCD at zero and at finite temperature from the lattice*, *Phys. Rev. D* **86** (2012) 094512 [arXiv:1209.6015] [INSPIRE].

[54] C. McNeile et al., *Direct determination of the strange and light quark condensates from full lattice QCD*, *Phys. Rev. D* **87** (2013) 034503 [arXiv:1211.6577] [INSPIRE].

[55] B.L. Ioffe, *Condensates in quantum chromodynamics*, *Phys. Atom. Nucl.* **66** (2003) 30 [hep-ph/0207191] [INSPIRE].

[56] V.M. Belyaev, V.M. Braun, A. Khodjamirian and R. Ruckl, *$D^*D\pi$ and $B^*B\pi$ couplings in QCD*, *Phys. Rev. D* **51** (1995) 6177 [hep-ph/9410280] [INSPIRE].

JHEP09(2021)023